

USING THERMAL PROFILING TO MONITOR  
OPTICAL FEEDBACK IN SEMICONDUCTOR LASERS

Evelyn W. Kapusta  
under the advisement of Dr. Janice Hudgings  
May 5, 2005

submitted to the faculty  
of Mount Holyoke College  
in partial fulfillment of the requirements  
for the degree of  
Bachelor of Arts with Honors

**TABLE OF CONTENTS:**

LIST OF FIGURES: .....	v
LIST OF TABLES:.....	viii
ACKNOWLEDGMENTS:.....	ix
ABSTRACT: .....	x
<b>Chapter 1 – INTRODUCTION</b> .....	<b>1</b>
<b>Chapter 2 – BACKGROUND</b> .....	<b>4</b>
2.1 – Semiconductor Physics .....	4
2.1.1 – Edge Emitting Semiconductor Lasers (EEL) .....	5
2.1.1.1 – Gain Mechanism .....	6
2.1.1.2 – Fabry-Perot Resonator.....	12
2.1.1.3 – Mirrors.....	16
2.1.2 – Vertical Cavity Surface Emitting Lasers (VCSELs) .....	19
2.2 – Optical Feedback.....	20
2.2.1 – Effects of Optical Feedback .....	21
2.2.1.1 – The Effect of Optical Feedback on the Spectral Characteristics of an EEL (The 5 Regimes) .....	22
2.2.2 – Uses of Optical Feedback.....	28
2.2.4 – Quantifying Optical Feedback.....	28
2.3 – Thermal Profiling .....	29

2.3.1 – External Heat Exchange Model.....	29
<b>Chapter 3 – THE EXPERIMENTS.....</b>	<b>34</b>
3.1 – Experimental Setup .....	34
3.2 – Experimental Setbacks and Solutions.....	39
3.2.1 – Thermocouples .....	39
3.2.2 – Laser Issues .....	40
3.2.3 – Back reflected Light striking the Thermocouples .....	42
<b>Chapter 4 – RESULTS .....</b>	<b>45</b>
4.1 – Quantifying the Shift in Threshold Current using Thermal Profiling .....	45
4.2 – Predicting Optical Output Power from Thermal Measurement .....	49
4.2.1 – Modification of External Heat Exchange Model to account for Optical Feedback.....	50
4.2.2 – Calculating Thermal Impedance ( $Z_t$ ) .....	51
4.2.3 – Direct optical measurement of Optical Output Power ( $P_{out}$ ).....	52
4.3 – Quantifying Optical Feedback with various amounts of Optical Feedback .....	54
4.4 – Solving for the Couple Efficiency ( $\rho$ ) .....	58
<b>Chapter 5 – CONCLUSION.....</b>	<b>61</b>
<b>Appendix A – Thermocouple Construction Guide .....</b>	<b>63</b>
A.1 – Thermocouple Construction.....	64
A.2 – Tip Technique.....	67
A.3 – Application of Electrical Insulation.....	69

A.4 – Thermocouple Testing ..... 71

REFERENCES: ..... 73

## LIST OF FIGURES:

Figure 1 - Typical EEL construction – Figure taken from [7].....	5
Figure 2 - Silicon Crystal Lattice – Figure taken from [7].....	6
Figure 3 - Doped Crystal Structure containing a free electron – Image Taken from [7] .....	7
Figure 4 - Energy Band Diagram.....	8
Figure 5 - Photon Production & Destruction – Image taken from [7].....	10
Figure 6 - Typical Gain Spectrum .....	12
Figure 1 – Current versus Output Power (LI).....	12
Figure 8 - Fabry-Perot Resonator .....	13
Figure 9 - Standing Waves within a Fabry-Perot Resonator.....	13
Figure 10 - Ideal Frequency Spectrum of Fabry-Perot Cavity .....	14
Figure 11 – Laser Frequency Spectrum .....	15
Figure 12 - Lasing Spectrum with Loss .....	16
Figure 13 - Reflection and Transmission at a Surface .....	17
Figure 14 – VCSEL – Figure taken from [13].....	19
Figure 15 – Typical Emission Spectrum for EEL without Feedback .....	22
Figure 16 - Emission Spectrum – Feedback Regime I.....	23
Figure 17 – External Cavity Modes - Feedback Regime II.....	24

Figure 18 - Emission Spectrum - Feedback Regime III.....	25
Figure 19 - Emission Spectrum - Feedback Regime IV .....	25
Figure 20 - Decreased Loss in a system under the influence of optical feedback.....	26
Figure 21 - LI Curve with and without Optical Feedback .....	27
Figure 22 - Temperature vs Input Power .....	31
Figure 23 –Theoretical IV' vs $\Delta T - \Delta T_0 \left( \frac{T_{surf} - T_{amb}}{(T_{surf} - T_{amb})_0} \right)$ .....	33
Figure 24 – Example of the Laser use in our Experiment – Figure taken from [13] .....	35
Figure 25 - Experimental Setup #1 .....	35
Figure 26 - Experimental Setup #2.....	36
Figure 27 – Detail of a Mirco-thermocouple.....	37
Figure 28 - Actual Micro-Thermocouple compared to a Human Hair .....	38
Figure 29 - Experimental Placement of Thermocouples.....	38
Figure 30 – Change in Temperature vs Current when the thermocouples are picking up a current off the laser surface and shorting out the temperature box.....	40
Figure 31 - Side Mounted p-side up Lasers .....	41
Figure 32 - Extreme Excess heating above threshold due to back scattering light striking the Thermocouples .....	43
Figure 33 - Detail of back reflected light's affect on the laser surface .....	44

Figure 34 - Change in Temperature vs Electrical Power for the without Feedback Case .....	45
Figure 35 - Change in Temperature vs Electrical Power .....	46
Figure 36 - Deviation from the Linear Fit - With and Without Feedback .....	47
Figure 37 - Optical Output Power vs Electrical Input Power.....	48
Figure 38 - Calculations for the Thermal Impedance of laser #2 .....	52
Figure 39 - Calculated Optical Output Power vs Direct Optical Measurements...53	
Figure 40 - Optical Output Power vs Electrical Input Power for various amounts of Optical Feedback .....	55
Figure 41 - Change in Temperature vs Electrical Input Power for various amounts of Optical Feedback .....	56
Figure 42 - Deviation from the Linear Fit vs Electrical Input Power for Attenuator #2 .....	57
Figure 43 - Using the feedback ratio to solve for $\rho$ .....	59
Figure 45 - Thermocouple Wires.....	64
Figure 46 - Bare Micro-thermocouple .....	65
Figure 47 - Thermocouple Wrappings .....	66
Figure 48 - Soldering Junction Protection.....	66
Figure 49 - Thermocouple on a Micro-Positioner .....	67
Figure 50 - Schematic of Tip Creation.....	68
Figure 51 - Application of Super Glue.....	69
Figure 52 – Probe used to test Thermocouple Resistance .....	70

**LIST OF TABLES:**

Table 1 – Observed Threshold Input Powers .....	48
Table 2 – Attenuator Transmission & the Effective Reflectivities Values.....	54
Table 3 – Observed Threshold Currents with Attenuators.....	57

## ACKNOWLEDGMENTS:

When I arrived at Mount Holyoke College, I was the firstie who had no idea what was going on in Physics 115 or 216. I lived in office hours and clinic, but I was inspired by an upper classman who seemed to have similar issues with class, yet was able to excel in the research laboratory. That woman was Phoebe A. Judge, and I would like to thank her for laying the path for me to follow.

Most importantly I would like to thank my research advisor Dr. Janice Hudgings. She is my mentor, and a woman I will always look up to.

Thank you to Dr. Dietrich Lürßen. He showed me that it is possible to be wildly successful, while still having time for yourself and your family. The balance he has achieved in his life is something I hope to achieve.

To my friends of all disciplines, thank you for keeping me sane during the thesis process. Special thanks to Amanda Dubs for sitting through the physics discussions you hardly understood, the tears, and denial. But most of all for being one of the best friends a person could ask for. To Rhea Ghosh and Emily Jones for long walks, chai, and thesis dates.

Thank you to my family - Mom, Dad, and Ann - for their continual support and belief in me. Follow what makes you happy.

Thank you to the people who sat in the dark windowless lab in the basement of Shattuck with me – the Optoelectronics Lab Group at MHC. Thank you to Eliz for the laughs, to Preema for the support, to Zariat for running data at 3am, to Whitney for the hugs, and Reja for being the other crazy senior writing a thesis in Janice's lab. But most of all thank you and good luck to Liz Merritt, the next senior lab rat. I know that you will do amazing things.

Thank you to the Department of Physics at Mount Holyoke College, without the support of all the faculty and staff, I never would have made it this far. Especially to Cindy, who helps keep this department of absentminded physicists in line.

Thank to the golf team and especially coach Shawn Durocher, who still let me play even after all the time I spent in lab and at conferences. A special heartfelt thank you to Kara Solem, who continually supported and reminded me that it was ok to spend my time doing what I love.

**ABSTRACT:**

Over the past several decades, it has been firmly established that edge-emitting semiconductor lasers are particularly sensitive to optical feedback. A semiconductor laser acting under the influence of optical feedback can result in any number of negative effects including mode hopping, coherence collapse, strong excessive noise, and chaotic dynamics [3]. Fortunately, we know that the amount of optical feedback can be quantified by examining the shift in threshold current, and redshifting in the lasing wavelength [1,2]. Although easily applied in open air systems, these techniques can not be used for circuits lacking direct optical access – such as photonic integrated circuits (PIC). Due to the semiconductors prominent use in PICs it has become apparent that a technique for quantifying optical feedback which does not require direct optical access is essential. In this work, we prove that through the precise monitoring of thermal conditions surrounding a semiconductor laser we can accurately quantify the amount of optical feedback without the necessity of direct optical measurements.

We examined the surface temperature ( $T_s$ ), heat sink temperature ( $T_{hs}$ ), and ambient temperature ( $T_a$ ) of a 5 quantum well InGaAsP/InP cleaved-facet laser coupled to a 38 cm long external optical cavity using  $25 \times 25 \mu\text{m}^2$  NIST-traceable

micro-thermocouples. We combined our experimental measurements with a total energy balance model for the laser:

$$P_{\text{rad}} = P_{\text{el}} - P_{\text{cond}} - P_{\text{conv}} = IV' - (T_s - T_{\text{hs}})/Z_T - A_{\text{eff}}h(T_s - T_a) \quad (1)$$

The electrical power ( $P_{\text{el}}$ ) generated in the laser is dissipated through conduction ( $P_{\text{cond}}$ ), convection ( $P_{\text{conv}}$ ), and radiative power ( $P_{\text{rad}}$ ) due to photons emitted by the laser [12]. The thermal impedance  $Z_T=15.0\text{K/W}$  and area-weighted heat transfer coefficient  $A_{\text{eff}}h=2.8\text{mW/K}$  were determined experimentally while operating the laser below threshold.

When the laser is exposed to optical feedback, a fraction  $\rho$  of the reflected light is coupled into the lasing mode, while the remaining fraction  $(1-\rho)$  is absorbed at the facet. Thus, the radiated power is:

$$P_{\text{rad}} = P_{\text{out}} - P_{\text{out}}R_{\text{ext}}(1-\rho) \quad (2)$$

where  $P_{\text{out}}$  is the optical power emitted and  $R_{\text{ext}}=91\%$  is the reflectivity of the external cavity.

Monitoring the measured difference,  $T_s - T_{\text{hs}}$ , as the bias current to the laser was increased, we observed the expected rise in the surface temperature proportional to the electrical power below threshold with  $P_{\text{rad}}=0$ . Above threshold, reduction in the slope occurs as emitted photons remove energy from the laser [12]. Through a close observation of this data we were able to determine the threshold current for various attenuation of the optical feedback. These threshold currents were then used to solve for the coupling efficiency ( $\rho$ ) of the back reflected light which is attempting to reenter the lasing cavity.

Using equation 1 and 2 and our temperature measurements alone, we were able to find the optical output power emitted by the laser without recourse to direct optical measurements. From these optical output powers we were then able to quantify the amount of optical feedback affecting the laser by examining the shift in threshold current [1].

Ultimately, we provide various methods for quantifying optical feedback through the close observation of the thermal measurements taken on and around a typical edge-emitting semiconductor laser. Comparing the results from our proposed thermal method and the traditional direct optical measurements, we found a strong quantitative agreement for both cases, with and without feedback.

## Chapter 1 – INTRODUCTION

LASER is an acronym for *l*ight *a*mplification by *s*timulated *e*mission of *r*adiation. Lasers come in a wide variety of shapes, sizes, and forms. There are solid state lasers and gaseous lasers, lasers a few atoms thick and three stories tall, each built of different materials and used for a different purpose. To children of the 90s, lasers signify a world of fantasy where aliens shoot them out of UFOs, Darth Vader uses them to blow up Alderaan in *Star Wars*, and Dr. Evil attaches them to the head of sharks in *Austin Powers*.

In all seriousness the strength of lasers lies in their versatility. Lasers can be found in CD and DVD players and laser printers. They are used in the grocery store to read bar codes and in outer space to scan the exterior of the space stations. Lasers are used in surgery for precision cutting around the heart and within the eye. They are also used by the military for missile tracking and in rifle scopes. However, the today's most common use of lasers is in communications.

Currently the telecommunication industry uses pulsating lasers to produce digital signals in the form of light waves. The most commonly used laser in telecom is the edge-emitting semiconductor laser. The laser generated signal is

coupled into a network of fiber optic cables that is used to carry the signal around the world. In order to control and protect the data stream throughout the journey, the beam of light passes through a variety of optical devices, including optical amplifiers and multiplexers. In order to simplify the installation of these complex circuits, engineers strive to miniaturize and integrate the circuits into a single chip, a *photonic integrated circuit* (PIC). PICs provide a number of advantages for the telecom industry including a smaller footprint, reduced cost, and simplified optical alignment.

In addition to all of the PIC's advantages, their small size produces a number of less desirable consequences. One of the largest problems lies in PIC debugging. Traditional optical debugging techniques involve placing a device for measuring beam characteristics at various places within the free space optical network in order to observe the output power, wavelength, and mode at that point. The typical PIC is about the size of your fingernail while a typical photo-detector or spectrometer can be as small as a can of tuna up to the size of a VCR, making it difficult to fit them between the components of the PIC. Additionally, the light beams within a PIC travel from device to device through a series of interconnected waveguides, eliminating open air pathways and the use of typical debugging techniques. Therefore, when a PIC chip begins to malfunction engineers simply replace the entire chip.

There are a number of effects that can cause an optical circuit to malfunction; one of the most common and destructive is optical feedback.

Optical feedback is the term used to describe the phenomenon of light being reflected off a surface back into a laser or other optical device. Previous investigations have shown that a laser under the influence of optical feedback will show a shift in the initial lasing point [1] and wavelength [2], eventually leading to coherence collapse and chaotic behavior [3,4]. These characteristics are commonly quantified by using a photo-detector or spectrometer, devices we already know can not be used for PIC debugging.

Over the last two years, our lab has been exploring the possibility of using thermal measurements as a noninvasive technique for measuring the presence of optical feedback within an optical circuit. By studying the change in temperature along the top of an edge-emitting semiconductor laser for varying amounts of optical feedback, we provide a solid argument for the use of thermal profiling for optical feedback debugging in PIC and other complex optical circuits.

In the following chapter we will lay the foundation for our work by establishing a good understanding of edge emitting semiconductor lasers, optical feedback, and thermal profiling through the inspection of previous work in these fields. In chapter 3 we begin looking at our experiment in particular, including our experimental techniques and setbacks. Data and results are presented in chapter 4. Finally, in chapter 5, we will look ahead to future projects resulting from the success of our work.

## Chapter 2 – BACKGROUND

### 2.1 – Semiconductor Physics

According to Merriam Webster’s dictionary, a laser is defined as “a device that utilizes the natural oscillations of atoms or molecules between energy levels for generating coherent electromagnetic radiation usually in the ultraviolet, visible, or infrared regions of the spectrum [5].” This definition illustrates the complexity of the laser while highlighting all of its essential elements – the most important being the resulting beam of “*coherent* electromagnetic radiation”. A perfectly coherent electromagnetic wave consists of photons with identical wavelengths (monochromatic), phase, and direction. Unfortunately a perfectly coherent beam is not a realistic possibility. A perfectly monochromatic beam is impossible due to the noise introduced by spontaneous emission, while directionality will be upset by diffraction at the laser facet [6]. Nevertheless it is important to remember that the defining aspect of laser science lies in the fact that we are able to produce a beam with a relatively narrow range of wavelengths, phases, and directions [6].

### 2.1.1 – Edge Emitting Semiconductor Lasers (EEL)

The basic edge-emitting semiconductor laser (EEL) design consists of a carefully constructed crystal lattice which is bonded to contact pads for electrical input.

The crystal is divided into three major regions: the p-cap, active region, and n-substrate, as shown in Figure 1.

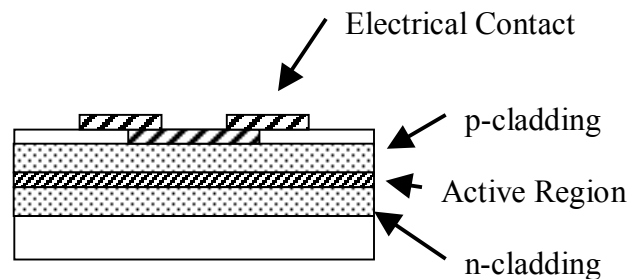


**Figure 1 - Typical EEL construction – Figure taken from [7]**

Each of these regions is composed of a slightly different crystalline structure in order to promote electron movement caused by their varying band gap energies, which eventually results in photon production. The differing crystalline composition of the p and n regimes results in different indices of refraction, causing the produced photons to be confined to the active region. Therefore, a highly efficient EEL must consist of elements which form the proper band gap energy to produce photons and elements that will confine the photons because of their respective indices of refraction [6, 7].

### 2.1.1.1 – Gain Mechanism

Now let us take a closer look at the actual mechanics behind photon production. We begin with a discussion of atomic energy levels. With a clear understanding of energy levels in place, one can begin to understand the properties of insulator, conductors, and semiconductors. From there one can explore the phenomena of spontaneous emission, stimulated emission, and stimulated absorption – the keys to photon production within a laser.

It all starts in the EEL's crystalline structure. The EEL crystal is composed of carefully selected atom combinations. Each atom is surrounded by a cloud of electrons which are arranged into discrete energy levels according to their unique characteristics.

Consider the element silicon, which contains four electrons in its outermost orbital, or valance shell. The atoms bond in order to fill their valance shell. In silicon's case a full valance shell contains 8 electrons. Therefore if a silicon atom shares one of its electrons with four other silicon atoms, all of the surrounding atoms will have full shells, forming a tight lattice like the one shown in Figure 2.



Figure 2 - Silicon Crystal Lattice – Figure taken from [7]

This structure is great for silicon but bad for electron movement. Therefore scientists replace one of the silicon atoms with an element containing one more or one less electron than silicon, such as phosphorus and gallium; this process is known as doping. If we dope silicon with an element containing five electrons in its valance shell, we introduce free electrons to the system and create a n-type material (Figure 3). On the other hand if we dope silicon with an element with three electrons in its valance shell we create a positively charged lattice containing “holes” (carriers or missing electrons) which we define as a p-type material.

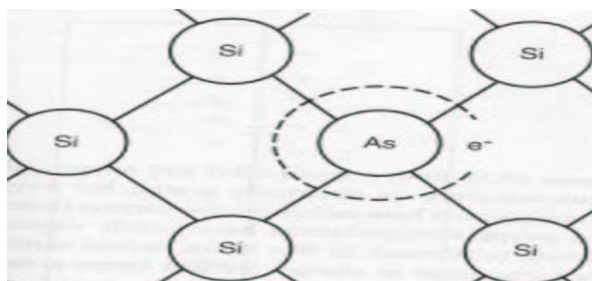


**Figure 3 - Doped Crystal Structure containing a free electron – Image Taken from [7]**

These n-type and p-type lattices are the crystals that make up the n-type and p-type regions of our EEL. By placing these materials beside one another, scientists have created a crystal structure which allows for easy electron movement. By separating the p-n junction by a thin non-doped material the scientists create a region where the electron movement and in turn photon production can be contained and controlled. We call this the active region.

Since we wish to focus on electron movement, we can simplify our model into the discrete energy levels through which electrons are moving: the valance and the conduction bands. The amount of energy required to move an electron from the valance band to the conduction band is called the band gap energy,  $E_g$ , which is determined by the materials electronic potential and the Schrödinger wave equation [7]. Visually we can represent this as shown in Figure 4.

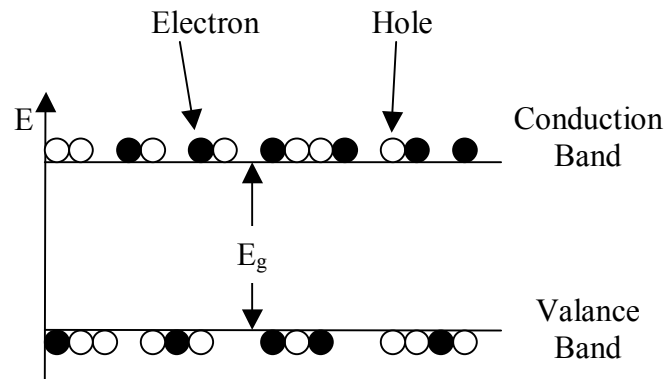


**Figure 4 - Energy Band Diagram**

At this point we have simplified the complicated atomic structures to an energy level diagram consisting of the valance and conduction bands with a given  $E_g$  for the particular atomic structure. With our energy diagram in place we can easily examine the complex electron movement that is the foundation of lasing action.

There are three basic types of materials – insulators, conductors, and semiconductors. An *insulator* is defined by a valance band full of electrons and a conduction band full of holes at the temperature absolute zero, separated by a large band gap energy. These properties make it nearly impossible for electrons to jump from the valance to conduction band energy even when energy is added to the system in the form of heat, current, or injected light. A *conductor*, on the other hand, has a small band gap energy and a practically full valance band, allowing it to contain both electrons and holes, as seen in Figure 4. In this system even small amounts of thermal energy will cause electrons to jump levels because of the small band gap energy and the available space for electron movement within the valance and conduction band. A *semiconductor* is a combination of the two; like the insulator, the valance band in the semiconductor is full at absolute zero, leaving no place for electrons in the conduction band to jump to. However, like a conductor, it possesses a small band gap energy allowing for easy electron movement with small amounts of external energy.

As an electron moves from one energy band to the other there must be a transfer of energy equal to the band gap energy,  $E_g$ . In lasers, this energy appears in the form of photons.

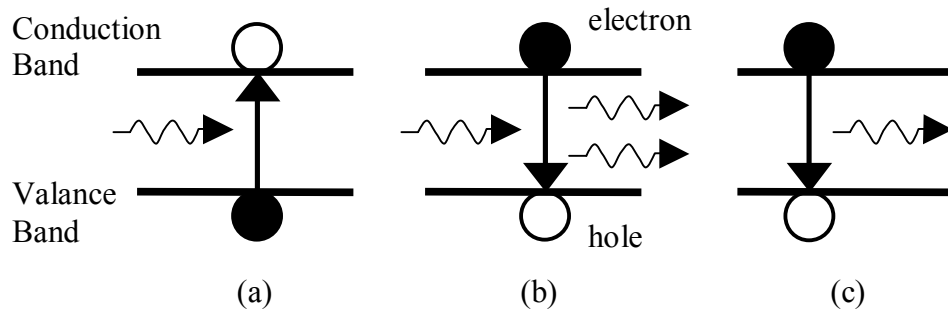


**Figure 5 - Photon Production & Destruction – Image taken from [7]**

Consider Figure 5; as a photon with energy  $E_\lambda$  approaches an electron configuration with a matching band gap energy (eg  $E_\lambda = E_g$ ), one of two things will happen. If there are a large number of electrons in the valance band, an electron can jump from the valance band to conduction band absorbing the initial photon – or *stimulated absorption* (Figure 5a). This process requires that the photon energy,  $E_\lambda$ , is equal to the band gap energy,  $E_g$ , so that energy is conserved. On the other hand, if there are a large number of electrons in the conduction band, the photon can stimulate an electron to fall from the conduction band to the valance band, producing an additional photon which is identical in every respect (wavelength, phase, and direction) to the first. This process is *stimulated emission* (Figure 5b) and is the essential component of laser gain. Occasionally in a system where the conduction band contains electrons and there is space (or holes) in the valance band, an electron may randomly fall from the conduction band to the valance band. This produces a photon whose energy matches the band gap energy of the system. This process is defined as

*spontaneous emission* and is shown in Figure 5c. Photons emitted by spontaneous emission have a wavelength fixed by the band gap energy, but have random phase and direction.

At this point one may be asking how are the electrons getting to the conduction band in the first place since at  $T=0$ , all of the electrons occupy the valance band. By applying an electrical bias (or current), the conduction band is loaded with electrons, increasing the probability of stimulated emission. When the probability of stimulated emission equals the probability of stimulated absorption, the system has reached the point of *transparent gain*. As the conduction band continues to be loaded with electrons, the system will pass the point of transparent gain and reach *carrier/population inversion*. At that point, the probability for stimulated emission is greater than stimulated absorption, creating a net gain (or photon production with in the cavity). The total amount of gain within the lasing cavity is quantified by the gain spectrum shown in Figure 6.

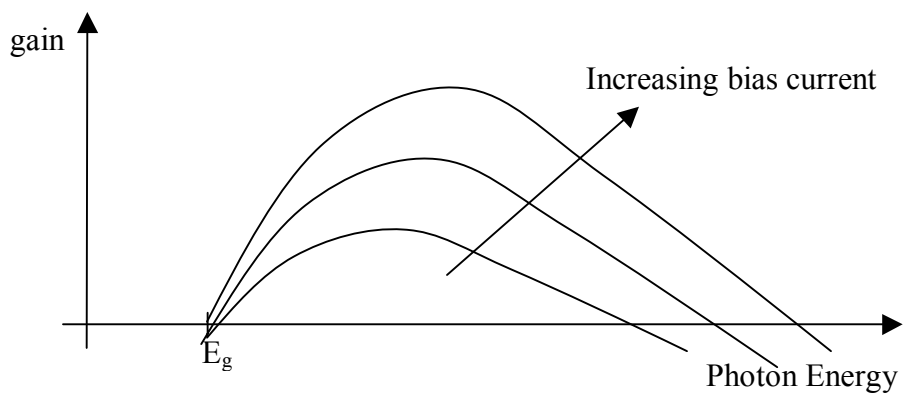


Figure 6 - Typical Gain Spectrum

Gain is increased through the addition of electrons to the conduction band. This is controlled experimentally with current. Therefore threshold, or the point when lasing begins, is thought of in terms of current. If we plot output power versus current, threshold is clearly visible, as pointed out in Figure 7.

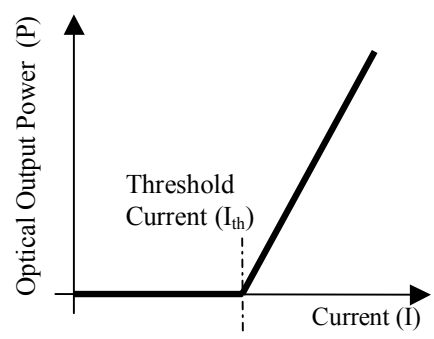
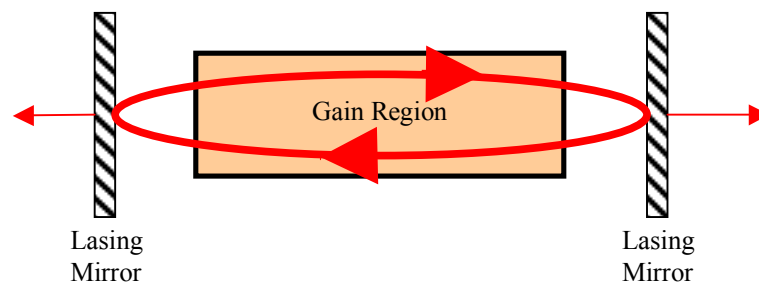


Figure 6 – Current versus Output Power (LI)

### 2.1.1.2 – Fabry-Perot Resonator

Laser action requires two events– a photon gain mechanism and internal optical feedback [6]. This is due to the fact that the number of photons created in a single pass through the active region will not be sufficient to create a visible lasing output (approx  $10^{19}$  photons) [6]. Therefore we need a mechanism that will allow

the photons to pass through the active region several times before being emitted. This is accomplished by the presence of a Fabry-Perot resonator cavity surrounding the gain region. A Fabry-Perot resonator is comprised of two highly reflective mirrors which allow small portions of light pass through, while reflecting the most of the light back through the active/gain region, where it can be further replicated through stimulated emission; as seen as Figure 8.



**Figure 7 - Fabry-Perot Resonator**

One interesting point to note is the fact that not all wavelengths are able to exist within the resonating cavity. Due to the cavity's structure, only wavelengths that contain a node at the end mirrors will not be destroyed by destructive interference upon back reflection. This creates standing waves similar to those shown in Figure 9.

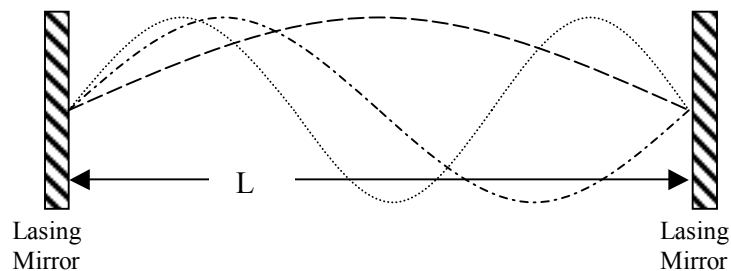


**Figure 8 - Standing Waves within a Fabry-Perot Resonator**

Knowing the total length of the lasing cavity ( $L$ ) we can solve for the allowed frequencies ( $f$ ) for a given laser using by relating the velocity of light within the lasing cavity,  $v$  to the wavelength of the standing wave ( $\lambda$ ) generated by the cavity length. To find  $v$ , the speed of light in a vacuum ( $c$ ) is divided by the index of refraction of the lasing medium ( $n$ ) in order to account for the lack of vacuum. The wavelength within the cavity is dependent on the length of the cavity ( $L$ ) and the modal number of the wave ( $N$ ).

$$v = \frac{c}{n} \quad (1)$$

$$\lambda = \frac{2L}{N} \quad (2)$$

Combining these elements we find that the space between frequencies is defined as:

$$\Delta f = \frac{v}{\lambda} = \frac{c}{2nL} \quad (3)$$

We can graph these frequencies against output power to easily view the possible frequencies for a given laser as shown in Figure 10.

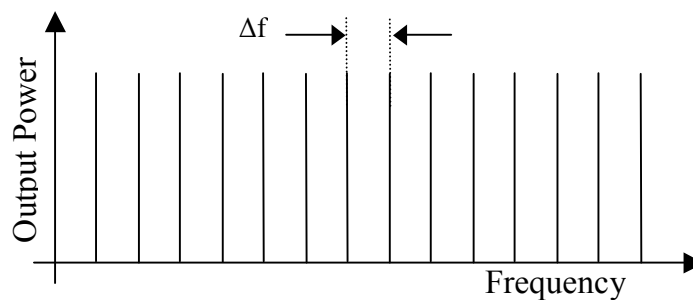


**Figure 9 - Ideal Frequency Spectrum of Fabry-Perot Cavity**

In the ideal case, in which there were no photons lost through the mirrors, the allowed resonator frequencies would appear as infinitely narrow spikes.

However, in the actual EEL frequency spectrum, the frequency spikes more closely resemble slight peaks with a finite width, since the reflective surfaces allow some light to pass through.

One way of looking qualitatively at the internal workings of the laser is to examine the gain spectrum combined with the Fabry-Perot resonator frequency graph. Plotting one on top of another, as seen in Figure 11, we see that certain frequencies experience more gain within the cavity due to the natural shape of the gain spectrum.

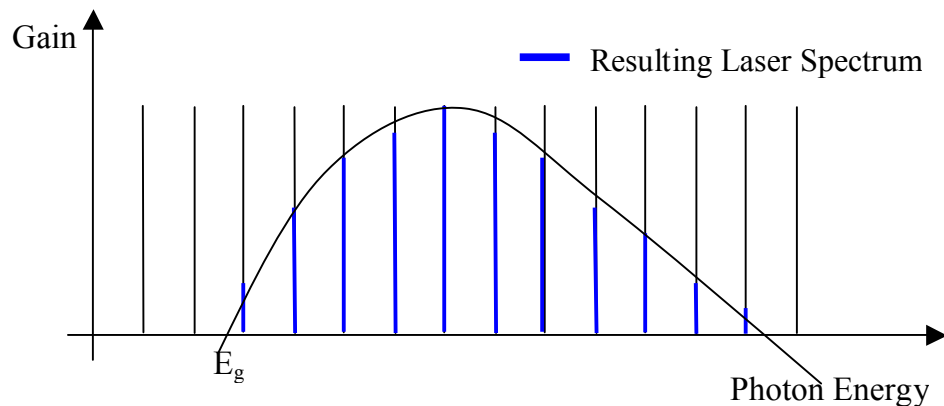


**Figure 10 – Laser Frequency Spectrum**  
**due to the combination of the gain spectrum + Fabry-perot frequencies**

This is important when we begin to look at the threshold current, the current at which lasing begins. You may recall that lasing only occurs when gain equals loss in the lasing cavity. Therefore, only the longitudinal modes which receive

enough gain to equal the loss will lase, while all others will die out due to natural losses within the cavity. This is shown schematically in Figure 12.

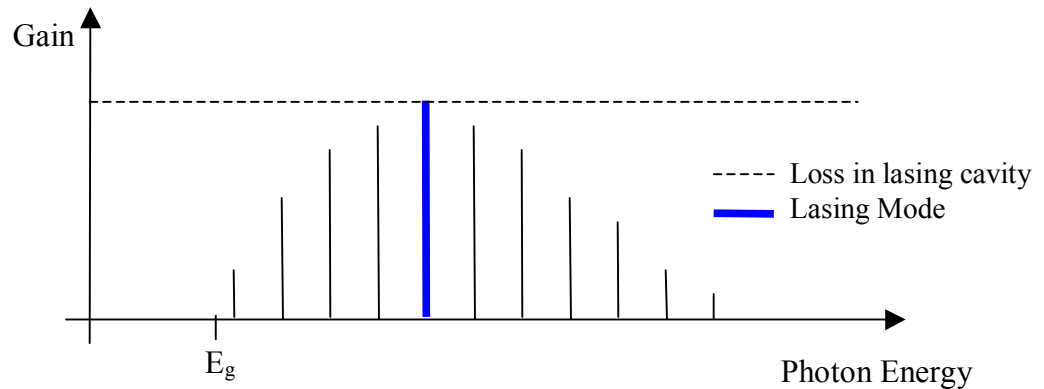


**Figure 11 - Lasing Spectrum with Loss**

Typically for a fixed amount of loss there is only one resonant mode that reaches the loss line, producing a monochromatic output beam. This explains why there is still a coherent output despite the presence of various Fabry-Perot frequencies. Our solid understanding of Figure 12 will be particularly helpful once we begin discussing the effects of optical feedback in the following section.

### **2.1.1.3 – Mirrors**

Another key principle of lasing operation is the mirrors' effect on the output beam. When an electromagnetic wave approaches a boundary between two materials of different refractive indices (Figure 13) such that the direction of propagation is perpendicular to the index boundary, the wave will be reflected according to the equation:

$$r = \frac{E_{refl}}{E_{in}} = \frac{n_1 - n_2}{n_1 + n_2} \quad (4)$$

$$t = \frac{E_{trans}}{E_{in}} = \sqrt{1 - r^2} \quad (5)$$

where  $r$  is the fraction of the incoming electromagnetic wave ( $E_{in}$ ) that is reflected back off the surface ( $E_{refl}$ ), and  $t$  is the fraction of the electromagnetic wave is the transmitted through the surface ( $E_{trans}$ ).

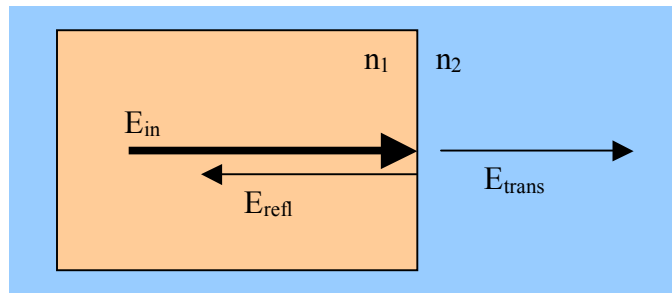


**Figure 12 - Reflection and Transmission at a Surface**

In EELs we can use equations 4 and 5 to determine the amount of photons that escape the lasing cavity to form the output beam. For a GaAs EEL in particular, the photons will pass from the lasing cavity with an index of refraction of  $n_1 = 3.6$  into the air, which has an index of refraction of  $n_2 = 1$ . By plugging these values into the equation 4 and 5 we find the field reflectivity,  $r = 0.56$  and  $t = 0.82$ . Therefore for every encounter at the lasing mirrors, 68% ( $T = t^2$ ) of the total power passes through the mirrors to create the output beam, while the other 32% ( $R = r^2$ ) is back reflected into the cavity to further stimulated emission.

One important thing to note about equation 4 is that when  $n_1 < n_2$   $r$  will be negative, which physically implies an  $180^\circ$  phase shift between the initial beam

and the back reflected one. Fortunately in EELs this is not a factor, since the beam is always going from a material of high refractive index (the laser material) to one a material of lower refractive index (air) [8].

At this point we have wholly discussed the various elements of EEL design and how each part affects the final coherent output. Unfortunately, the EEL structure is not flawless, and when combined with the production process, can result in a number of side effects. The first of these effects is relatively high cost (\$3-\$100/laser), due to the inability to test EELs before the final stages of production. During EEL production, the lasers are grown in long crystal strips that are then cleaved to form individual lasers, at which point they can be tested. Since there is no method for debugging until the lasers are cleaved, EEL production allows for a high percentage of loss, increasing production price. Secondly, due to the inability to shape the reflecting mirrors and asymmetric geometry of the active region, the output beam of an EEL is elliptical in shape with a slight divergence (10% or so) which must be corrected with a lens in order to obtain a cylindrical collimated beam. Thirdly, due to the location of the electrical connections and waveguides, EELs cannot be stacked to form 2D arrays.

Although these effects limit the effectiveness of EELs, laser science found a number of ways to work around them (which will not be discussed here) until an alternative could be made. This alternative was found in 1979 with the invention

of the vertical cavity surface emitting laser (VCSEL). Although it was invented in 1979, VCSELs did not become a mainstream component until they were able to produce threshold currents above 1mA in 1989.

### 2.1.2 – Vertical Cavity Surface Emitting Lasers (VCSELs)

Today VCSELs are rapidly acquiring a share of the semiconductor laser market.

The chief difference between VCSELs and EELs lies in the VCSEL's unique structure. The VCSEL's lasing cavity lies in the vertical plane, with the resonator mirrors located on the top and bottom of the device rather than on either side. A comprehensive diagram of a VCSEL can be seen in Figure 14 [6].

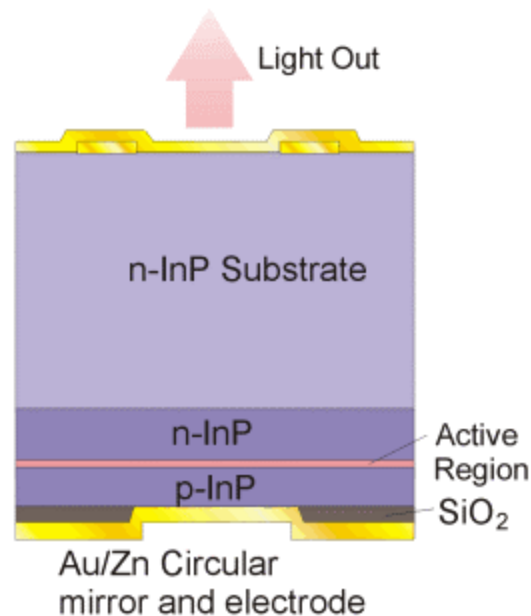


Figure 13 – VCSEL – Figure taken from [13]

Due to differences in structure, the VCSEL corrects for many of the imperfections in EELs mentioned in the previous section. During production each VCSEL is a separate entity, allowing for testing during production, decreased waste, and lower prices (less than \$1). Since the external mirrors are on the top and the bottom, the bottom mirror can be designed not to emit light (reducing loss out of that mirror), and the top mirror can be designed to minimize diffraction and is shaped to produce a circular beam (or any other shape for that matter). Stacking issues with EELs are also solved with VCSELs. Because VCSELs emit light vertically, they are easily grown in 2D arrays in the horizontal plane.

## **2.2 – Optical Feedback**

Now consider an EEL under the influence of optical feedback. As mentioned previously, optical feedback is defined as the “portion of the laser output [being] fed back into the laser cavity after reflection from an external mirror, grating, or fiber end [9].” Therefore by placing an EEL within an optical circuit we create an environment teeming with the potential for optical feedback from each optical surface. But is it really that bad? What will a little light reinjection do to the overall function of an EEL? That is what we are here to find out.

### **2.2.1 – Effects of Optical Feedback**

The laser was invented in 1960. Within the next 10 years, scientists had already begun to examine the effects of optical feedback, although it wasn't until 1981 that optical feedback research really took off. In that year a number of important papers were written by leading physicists in the field including L. Goldberg, K. Petermann, A. Olsson, and D. Lenstra [3,4,9,10]. After 20+ years of research, optical feedback is considered to be a well understood phenomenon in EELs.

Optical feedback has been shown to drastically affect the spectral characteristics of the output beam. How it affects the spectral characteristics is dependent on the amount of optical feedback present in the system. In order to simplify the discussion five specific feedback regimes have been defined for the various amounts of feedback and their corresponding spectral effects.

Before we look at each regime in detail, let's begin with a quick review of the spectral characteristics of EELs without optical feedback. Thinking back on our previous discussion, we remember that a laser will only lase once the laser has reached threshold current. This point is defined as the moment when the total gain within the lasing cavity is equal to the cavity losses from scattering at the mirrors, loss through the mirrors, and absorption due to material defects. This point can be visualized by examining the gain frequency spectrum graph (Figure 12), where a single peak represents the single lasing wavelength. Threshold is

defined as the current at which a single resonance frequency hits the loss line and lasing begins in that wavelength alone, also known as the dominant lasing mode. The lasing wavelength can be detected by spectral analysis and is commonly displayed as an emission spectrum (Figure 15).

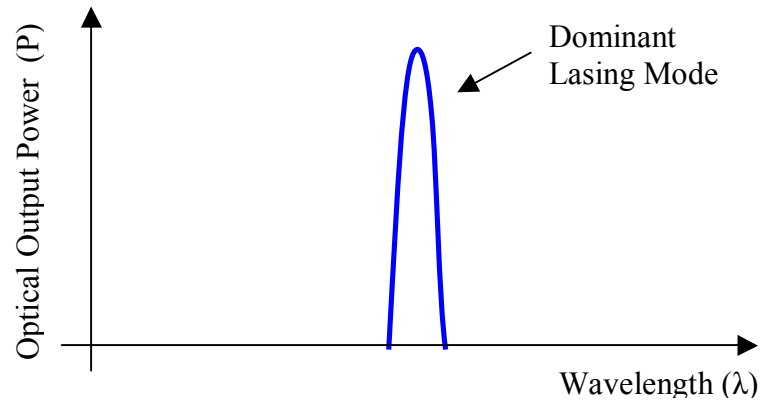


**Figure 14 – Typical Emission Spectrum for EEL without Feedback**

In this work, we shall refer to threshold *current* regularly although we define it in terms of power (IV). Threshold current can be found from the threshold power by dividing the power (IV) by the voltage (V).

### **2.2.1.1 – The Effect of Optical Feedback on the Spectral Characteristics of an EEL (The 5 Regimes)**

By introducing feedback to the system, we return some of the emitted photons to back into the lasing cavity. The returning photons have wavelengths matching those being produced within the lasing cavity; however their external trip has

caused a shift in phase. When the returning photons enter the cavity they will be replicated due to stimulated emission multiplying the number of photons with different phases. This appears in the emission spectrum as a broadening or narrowing of the dominant lasing mode depending on the returning phase of the photons, as shown Figure 16. This stage in optical feedback is known as feedback regime I [3].

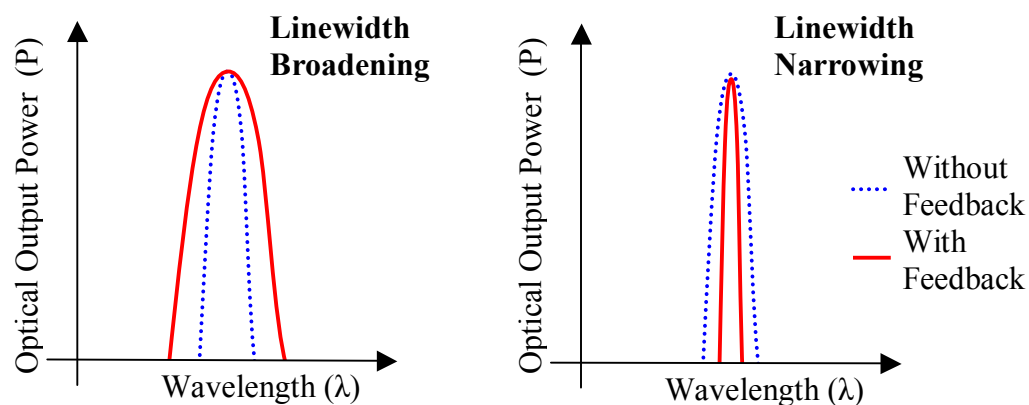


**Figure 15 - Emission Spectrum – Feedback Regime I**

As the optical feedback is increased, standing waves form between the external reflection mirror and the internal lasing mirrors known as external cavity modes. An example of these waves is shown in Figure 17. Initially these modes act as noise in the system but as more and more feedback is added to the system, the modes increase in strength appearing as tightly spaced additional frequencies. When the additional modes match the strength (or height) of the dominant lasing

mode, the laser will begin to jump between the lasing peaks causing the laser to run at various different wavelengths. This phenomenon is known as mode hopping (or frequency instability) and is the marker for feedback regime II. Although the laser is now lasing in various wavelengths over time (the effect of jumping between external cavity modes) it is still only lasing in a single wavelength at a time, thus remaining coherent [3].

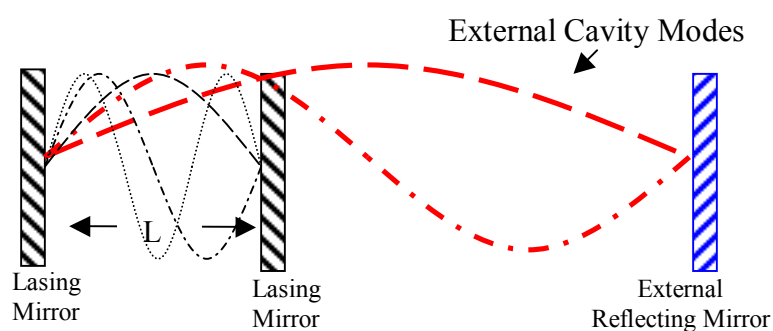


**Figure 16 – External Cavity Modes - Feedback Regime II**

In feedback regime III, the laser will begin to lase in the mode with the narrowest linewidth rather than the highest gain. This helps to restabilize the system after a sudden transition from the dominant lasing mode to one of the external lasing modes as they become narrower than the dominant peak. Feedback regime III is defined by the stabilizing lasing emissions, as shown in Figure 18 [9].

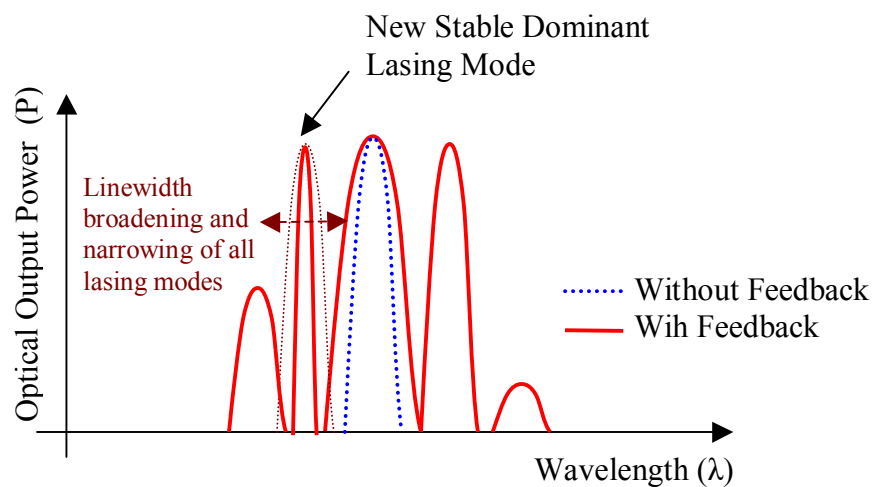


**Figure 17 - Emission Spectrum - Feedback Regime III**

If feedback is increased beyond the stability of regime III, we reach a point in which the multiple modes broaden to become a single envelope causing the laser to lase in multiple modes at once, depicted in Figure 19.

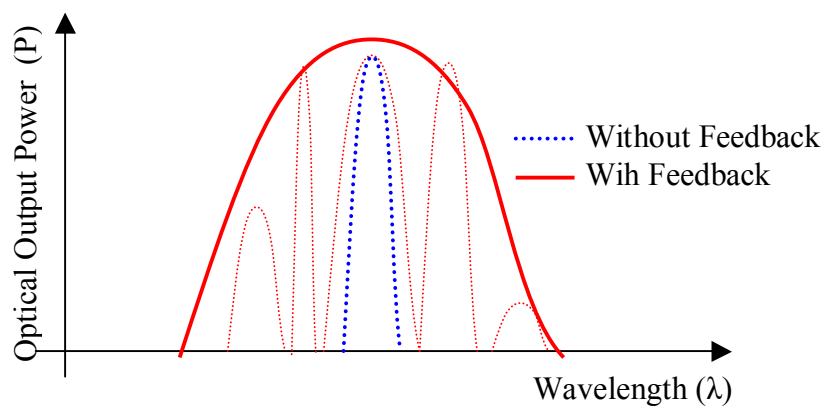


**Figure 18 - Emission Spectrum - Feedback Regime IV**

This sudden increase in linewidth is defined as coherence collapse, the characterizing factor of feedback regime IV. The amount of feedback required to create coherence collapse is defined as the critical feedback level. Coherence

collapse is the beginning of a string of events that completely nullifies the constructive use of the laser [3].

By increasing feedback further we enter feedback regime V, which is characterized by chaotic dynamics in the lasing emission due to the increased noise instabilities in the relaxation resonance frequency, the appearance of sub-harmonics, period-doubling and the frequency locking phenomenon [3]. These effects are studied in more detail in papers such as “Coherence Collapse in Single-Mode Semiconductor Lasers due to Optical Feedback” by Daan Lenstra [10].

### 2.2.1.2 – The Effect of Optical Feedback on Threshold Current

Beyond affecting the emission spectrum, optical feedback has also been shown to affect the threshold gain. As photons reenter the lasing cavity they will decrease the total loss within the cavity, as seen in Figure 20.

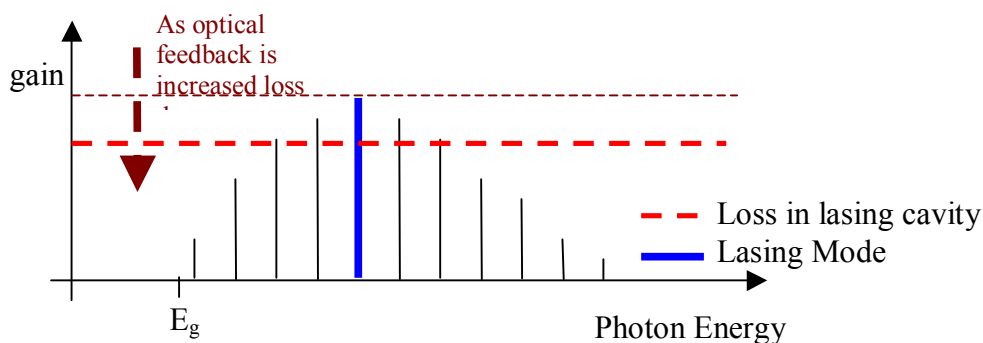
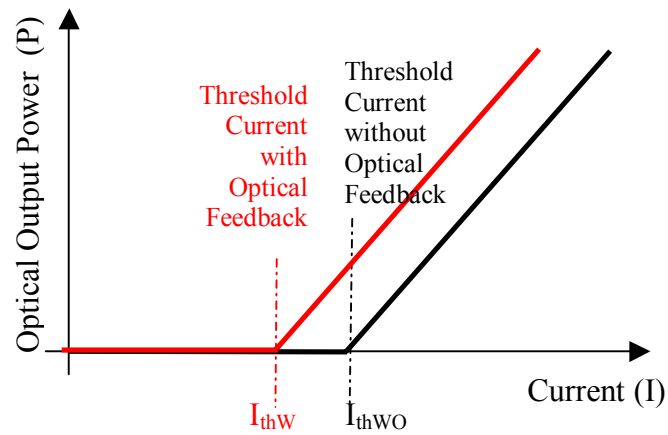


Figure 19 - Decreased Loss in a system under the influence of optical feedback

By lowering the amount of loss, we decrease the amount of gain required to match the loss, causing the laser to turn on earlier or lowering the threshold current, as shown in Figure 21.



**Figure 20 - LI Curve with and without Optical Feedback**

The amount of shift in threshold current is directly dependent on the total amount of optical feedback and can be modeled using equations original derived by A. Olsson and C.L. Tang in 1981, which were later simplified by S. Jiang in 1994. Below is the model presented by Jiang.

$$I_{th} = A \left( 2\alpha l + \ln \left( \frac{1}{R_1 R_{eff} T} \right) \right) \quad (6)$$

$$R_{eff} = \left[ \frac{\sqrt{R_2} + \sqrt{R}}{1 + \sqrt{R_2 R}} \right]^2 \quad (7)$$

In the equation,  $R_1$  and  $R_2$  are the reflectivities of laser end mirrors,  $R$  is the effective reflectivity of the external feedback cavity (which will be discussed in more detail in chapter 3),  $T=1-L_m$  where  $L_m$  is equal to the laser power loss within the EEL,  $l$  is the cavity length,  $\alpha$  is the absorption and scattering losses, and  $A$  is a proportionality constant [4,1]. Since we are working with EELs,  $L_m$  is very small, making  $T$  approximately equal to 1.

### **2.2.2 – Uses of Optical Feedback**

Although optical feedback eventually destroys laser coherence it can be used in measured amounts to control lasing output. It has been shown as an effective method for mode selection, narrowing of the emission spectrum, reduction of waveform distortion, electro-optical tuning, and self-pulsation [4,11].

### **2.2.4 – Quantifying Optical Feedback**

Traditionally the strength of optical feedback into a laser has been identified by directly observing the lasing output power using a photodetector or spectrometer in the beam path. PICs feature the optical components scaled down to nanoscale proportion and connected through integrated waveguides. Although PICs simplify installation and reduce cost, they increase debugging difficulty by decreasing size and removing all of the open air pathways. This in turn eliminates the use of photodetectors and spectrometers for characterization. With the rapid growth of these devices, it is becoming ever more important to find a way of quantifying

optical feedback without direct optical access. We hope to achieve this through a careful observation of fluctuations in the surface temperature of EELs with and without optical feedback.

### **2.3 – Thermal Profiling**

At this point, we have explored the properties of EELs with and without optical feedback. We have also discussed the inability to characterize PICs using traditional methods due to their size and lack of direct optical access. This underscores the importance of having an indirect, non-optical technique for characterizing optical feedback in lasers integrated into photonic circuits.

The aim of our research is to prove that optical feedback can be easily quantified using thermal measurements. Before we can do this, we must first establish a clear understanding of how temperature is related to the physical and spectral properties of EELs.

#### **2.3.1 – External Heat Exchange Model**

In April 2003, a team of researchers at the Massachusetts Institute of Technology (M.I.T.) constructed an accurate model of the external heat exchange for semiconductor laser diodes. In this section the findings of K.P. Pipe and R.J. Ram will be discussed in detail, since their work forms the basis of my research [12].

In our grade school physics classes, we learned that for a system in equilibrium energy must be conserved: power in = power out. Pipe and Ram used this basic principle when constructing their model.

In EELs the primary source of heating arises from joule heating created as an electrical bias current (I) is applied to the laser. This current is multiplied by the voltage (V) in order to be expressed as power ( $P_{el}$ ). Unfortunately, some of the input power is lost due to resistance (R) in the wire that carries the current to the laser. This term must be accounted for in our calculations, resulting in the following expression for total input power:

$$P_{el} = IV' = IV - I^2R \quad (8)$$

When considering output power, there are a number of mechanisms which removed energy from a laser: conduction ( $P_{cond}$ ), convection ( $P_{conv}$ ), and radiation ( $P_{rad}$ ). Both conduction and convection deal with the removal of heat through atomic vibrations. Conduction is typically seen in solids because heat is lost due to stationary atomic collisions. In contrast, convection is typically a liquid characteristic since heat is carried away through the 'translational motion of individual particles' [12]. The final mechanism by which heat is lost from a laser is through radiation ( $P_{rad}$ ). As photons leave the lasing cavity they take energy away from the device, decreasing the amount of energy left for convection and conduction, producing a measurable cooling. If we think about these three mechanisms graphically, as shown in Figure 22, we can see that before threshold we have a linear increase in temperature as electrical input power is increased.

Then when the laser turns on, the radiation removes energy from the system, which is seen as a sharp kink in the temperature measurements above threshold.

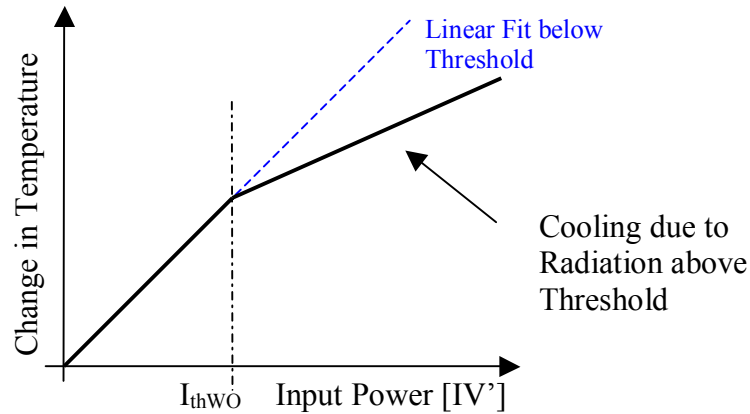


**Figure 21 - Temperature vs Input Power**

In EELs we see conduction as heat flow from the surface of the laser down to the heat sink, a device used to prevent laser overheating and extreme temperature fluctuations. Mathematically, conduction is simply the change in temperature divided by the device's geometrical impedance,  $Z_t$ .

$$P_{cond} = \frac{\Delta T}{Z_t} \quad (9)$$

where  $\Delta T$  is equal to the surface temperature minus the heat sink temperature ( $T_{surf} - T_{hs}$ ).

Convection is described as the amount of heat escaping off the top of the laser into the air. We quantify that by multiplying the surface temperature ( $T_{surf}$ ) minus the ambient temperature ( $T_{amb}$ ) by the surface area of the device ( $A$ ) and the heat transfer coefficient ( $h$ ). Unfortunately, due to lateral heat spreading the

heating area is not limited by surface area of the device. Therefore we must consider the effective area instead,  $A_{eff}$ . In the end the equation which describes convection is simply:

$$P_{conv} = A_{eff}h(T_{surf} - T_{amb}) \quad (10)$$

By combining equations (8), (9), and (10) and the fact that energy in equals energy out, we can construct the total energy balance equation.

$$P_{el} = P_{cond} + P_{conv} + P_{rad} \quad (11)$$

$$IV' = \frac{T_{surf} - T_{hs}}{Z_T} + A_{eff}h(T_{surf} - T_{amb}) + P_{rad}$$

In equation (11) all of the values except for  $Z_t$  and  $A_{eff}h$  can be determined through direct experimental observation.

$Z_t$  and  $A_{eff}h$  can be solved for experimentally by using equations (11) and setting the current to zero. In doing so can we find  $A_{eff}h$  in terms of  $Z_t$  and temperature.

$$A_{eff}h = \frac{\Delta T_0}{Z_t(T_{amb} - T_{surf})_0} \quad (12)$$

In this equation,  $\Delta T$  and  $(T_{amb} - T_{surf})_0$  are the values for the various temperature values when  $I = 0$ . By taking equation (12) and substituting it into equation (11) we can solve for  $Z_t$  in terms of experimentally measurable quantities.

$$Z_t IV' = \Delta T - \Delta T_0 \left( \frac{T_{surf} - T_{amb}}{(T_{surf} - T_{amb})_0} \right) \quad (13)$$

By plotting the right hand side of equation (13) versus  $IV'$ , we can get  $Z_t$  by finding the slope of the line below threshold, an example of such a calculations is shown in Figure 23. With a value for  $Z_t$  we can plug it into equation (12) and solve for  $A_{effh}$ .

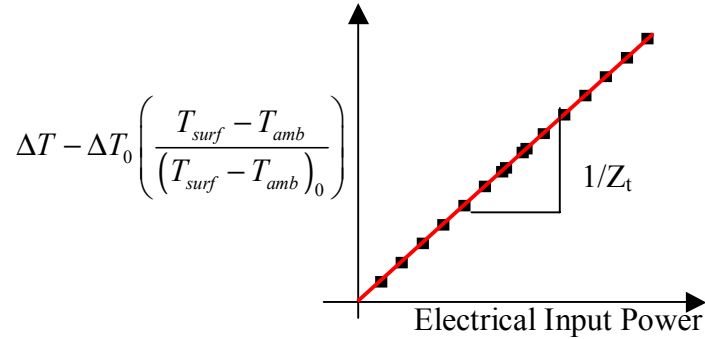


**Figure 22 –Theoretical  $IV'$  vs  $\Delta T - \Delta T_0 \left( \frac{T_{surf} - T_{amb}}{(T_{surf} - T_{amb})_0} \right)$**

At this point you may be asking, why are we only calculating  $Z_t$  below threshold? This is due to our definition of  $A_{effh}$ , where we have no optical output ( $P_{rad} = 0$ ), which only occurs below threshold. Therefore in our calculation of  $Z_t$  we must only observe the area below threshold.

With our values for  $Z_t$  and  $A_{effh}$ , in combination with our experimentally observed values ( $T_{surf}$ ,  $T_{hs}$ ,  $T_{amb}$ ), we have all of the components of the total energy balance equation (11) except for  $P_{rad}$ , our unknown. With the total energy balance equation in place, we can begin looking at our experiment in detail.

## **Chapter 3 – THE EXPERIMENTS**

### **3.1 – Experimental Setup**

The objective of our research is to observe the thermal effects of optical feedback on EELs. To do this we need to design a setup that contains a) a method for controlling the temperature around the laser, b) a feedback cavity with which we can control the amount of optical feedback being injected into the laser, and c) a method for measuring the temperature of the device (the thermal profiling setup). For our experiment in particular we are working with a multiple quantum well InGaAsP/InP cleaved-facet laser. This means we are working with a semiconductor laser with a ridge wave guide and multiple quantum wells within the active region. From here on we shall refer to this laser as laser #1, this laser would resemble the one shown in Figure 24.

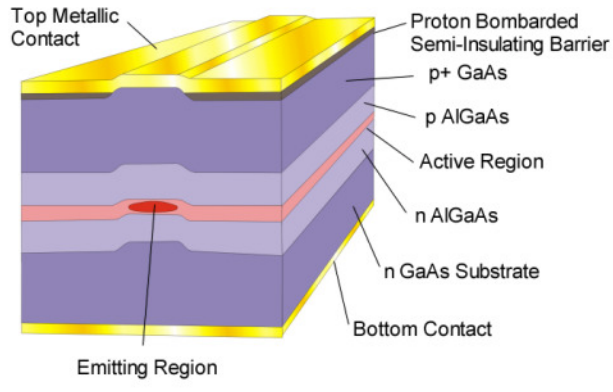


Figure 23 – Example of the Laser use in our Experiment – Figure taken from [13]

The laser is thermally controlled by a peltier cooler placed under a heat sink in order to prevent extreme temperature fluctuations. Throughout our experiments the heat sink temperature is set to 18° C.

Figure 25 shows a schematic of our experimental setup.

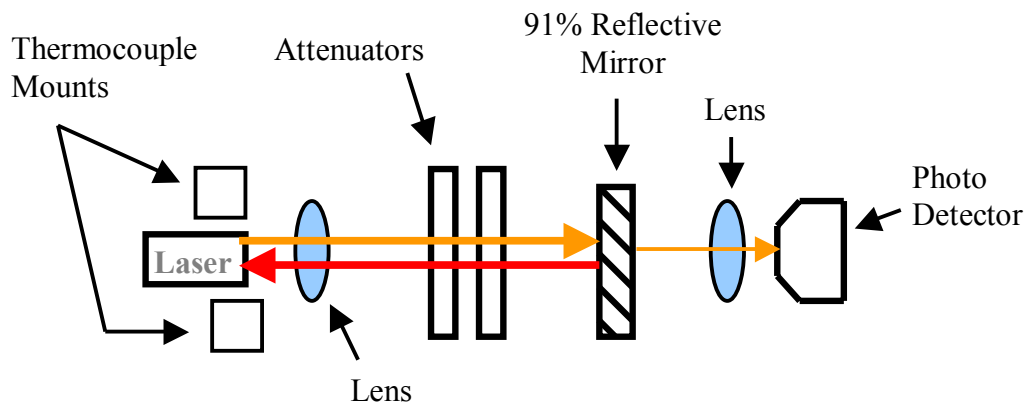


Figure 24 - Experimental Setup #1

Light that is emitted from the laser passes through a lens that collimates the beam. From there the light passes through a set of attenuators, used to control the

amount of optical feedback, to the 91% reflecting gold coated mirror. At this junction most of the light is back reflected into the laser forming our 38 cm feedback cavity. The remaining 9% of the light passes through the mirror and is focused with another lens before entering the photodetector.

During our time in lab we worked with another 5 quantum well InGaAsP/InP cleaved-facet laser with a gain peak at  $1.54 \mu\text{m}$ , which we call laser #2. We used laser #2 in an alternative setup in which a beam splitter was used to create the feedback cavity shown in Figure 26. In this setup the light is collimated at the first lens. At the beam splitter, half of the output beam passes straight through the beam splitter to the photodetector, while the other half is reflected upwards  $90^\circ$  towards a 99.8% reflecting mirror. The light incident to the reflecting mirror is back reflected into the beam splitter. At the beam splitter, the light is split again with half of it being directed towards the laser as optical feedback, and the other half being lost as excess. In this setup, only 25% of our total output beam is used for optical feedback.

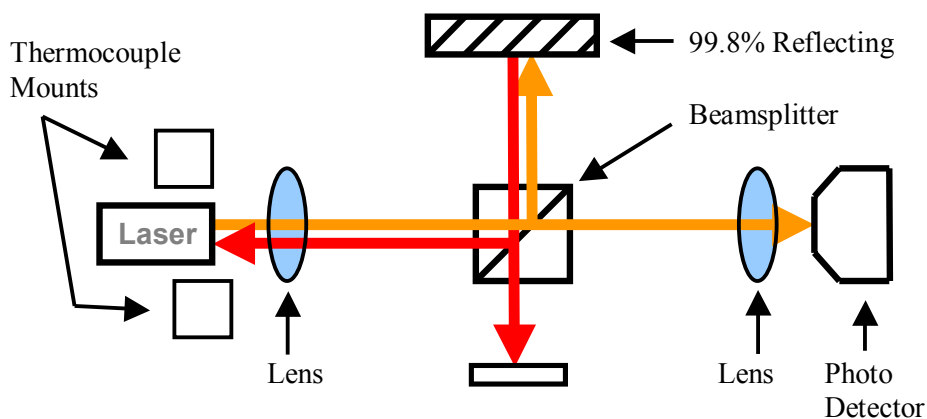


Figure 25 - Experimental Setup #2

Although we eventually abandoned this setup in order to increase the total amount of feedback (by switching to setup #1), it was used for a successful section of our project in which we were able to plot  $P_{\text{rad}}$  using our thermal calculations; this will be discussed further in the results section.

With our feedback cavity in place, we can now focus on our techniques for thermal profiling. Today one of the most common methods for noninvasive temperature measurements is the use of micro-thermocouples. A micro-thermocouple is made up of two small wires (typically copper and constantan) soldered together at the tip, as shown in Figure 27.

When exposed to a temperature, a voltage difference is generated between the wires according to the Seebeck Effect:

$$U = \gamma(\Delta T) \quad (14)$$

where  $U$  is the voltage difference and  $\gamma$  is the Seebeck coefficient. For our thermocouples in particular  $\gamma = -35$ . This conversion of voltage to temperature is easy thanks to thermocouple boxes which do the mathematical calculation automatically. In our experiment, we used three  $25 \times 25 \mu\text{m}^2$  NIST-traceable micro-thermocouples with an accuracy of 200 mK and a precision of 10 mK, depicted in Figure 28.

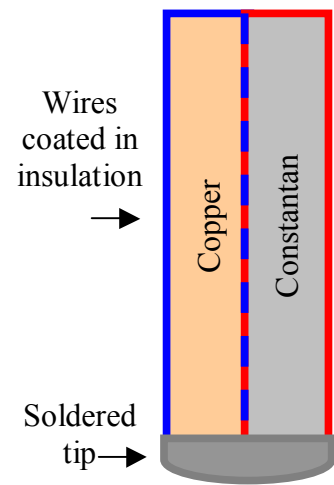


**Figure 25 – Detail of a Micro-thermocouple**

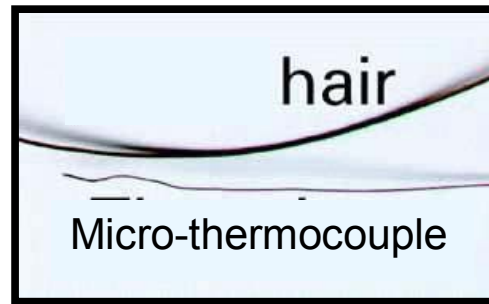


**Figure 26 - Actual Micro-Thermocouple compared to a Human Hair**

The placement of the micro-thermocouples used for our experiment is shown in Figure 29. One thermocouple was placed on the EEL ridge above the active region to measure surface temperature ( $T_{\text{surf}}$ ). One was placed on the heat sink surface to monitor changes in temperature ( $T_{\text{hs}}$ ). The final thermocouple hovered above the setup to monitor changes in ambient temperature ( $T_{\text{amb}}$ ).

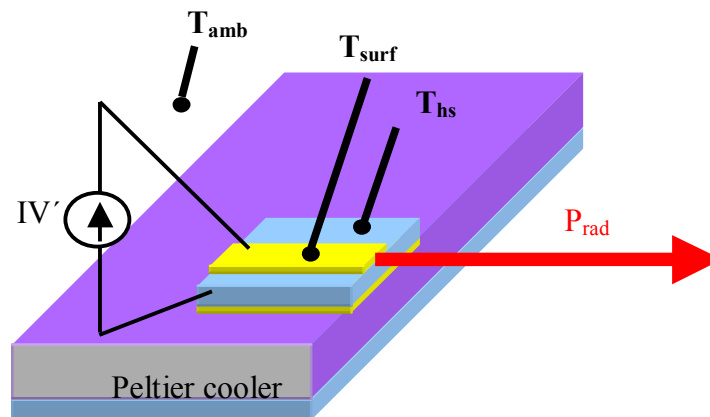


**Figure 27 - Experimental Placement of Thermocouples**

## **3.2 – Experimental Setbacks and Solutions**

In the process of conducting a successful experiment one runs into a number of problems that need to be solved before the project can move forward. Throughout the duration of this project we encountered three major issues – the thermocouples, laser selection, and back reflected light hitting the thermocouples.

### **3.2.1 – Thermocouples**

The first major issue we encountered involved the micro-thermocouples. For best results, the thermocouples must be calibrated to read within 0.1°C of each other on the same temperature controlled device. Since each thermocouple is soldered by hand in lab, we found this to be a challenging task. Finally, the issue was solved by perfecting a technique for thermocouple construction described in detail in Appendix A.

The second and more pressing issue encountered with the thermocouples involved them picking up the current running through the laser and shorting out the temperature box to which they were connected. This is clearly visible in the  $\Delta T$  graph shown in data Figure 30, when the heat sink thermocouple was picking up a current.

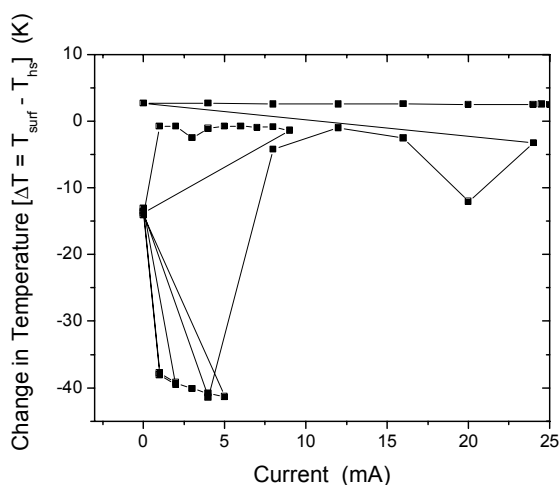


**Figure 28 – Change in Temperature vs Current when the thermocouples are picking up a current off the laser surface and shorting out the temperature box**

In order to prevent the effects seen in Figure 30, we had to insulate the tip of the thermocouple from the laser without decreasing the thermocouple's ability to detect temperature. Our solution was to coat the top of a thermocouple with a thin layer of super glue. Procedures for the application of super glue are also included in the thermocouple construction Appendix A.

### 3.2.2 – Laser Issues

In the world of lasers, there are various types of EEL. For our experiment, we needed to find an EEL which was arranged in order to maximize our temperature measurements by having heating elements within the device close to the laser surface.

Thinking back on our discussion of EEL construction we remember that an EEL consist of two major regions: the cap and substrate, which are either comprised of the positively (p-type) or negatively (n-type) doped materials. Due to the p-doped material's high resistance, large amounts of electrical heating occur in that region during lasing. In order to maximize cooling in the laser, EELs are usually mounted with the p-side adjacent to the heat sink. This arrangement is called p-side down. In order to achieve the clearest thermal measurements, we used a p-side up laser for our experiment, although this proved more challenging than it sounds.

In a number of cases, when we were able to find a p-side up laser, we found that they were either mounted poorly for cooling, or had such a low maximum output power that they did not produce sufficient cooling to be detected by our thermocouples. Most p-side up lasers we found were side mounted, as shown in Figure 31.

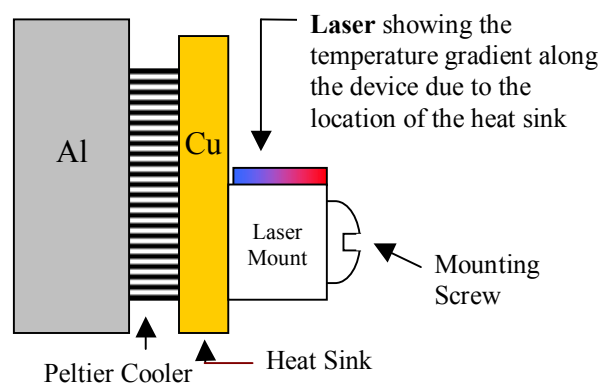


**Figure 29 - Side Mounted p-side up Lasers**

By mounting the lasers to the front of our heat sink we achieved uneven cooling along the device, producing much higher temperatures at the front of the device and skewing our data.

In the end we found that EELs consisting of p-side up configuration, which were mounted from below, while still processing a high optical output power, performed best for our experiment.

### **3.2.3 – Back reflected Light striking the Thermocouples**

Once we began taking data, we found that with feedback we were experiencing a large amount of additional heating above threshold as shown in Figure 32. As you may remember from our previous discussion, above threshold current we expect cooling due to the photon emission. The drastic increase in slope in the with feedback case implies excess heating above threshold.

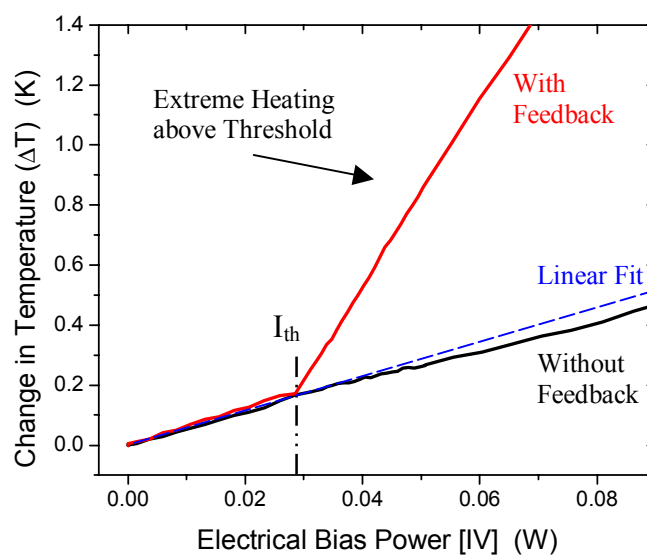


**Figure 30 - Extreme Excess heating above threshold due to back scattering light striking the Thermocouples**

When considering what was causing this extreme heating we had to consider how back reflected light effected the overall heating and cooling of the system. When back reflected light reaches the laser facet, the light has three options 1) to be coupled into the cavity as optical feedback, which increases the optical output power and eventually cools the system, 2) to be absorbed by the material surrounding the laser facet, increasing the external temperature, or 3) passing over the top of the laser. After some careful thought, we decided that this heating was caused by photons hitting the thermocouple as they passed over the top of the device face, as depicted in Figure 33(a).

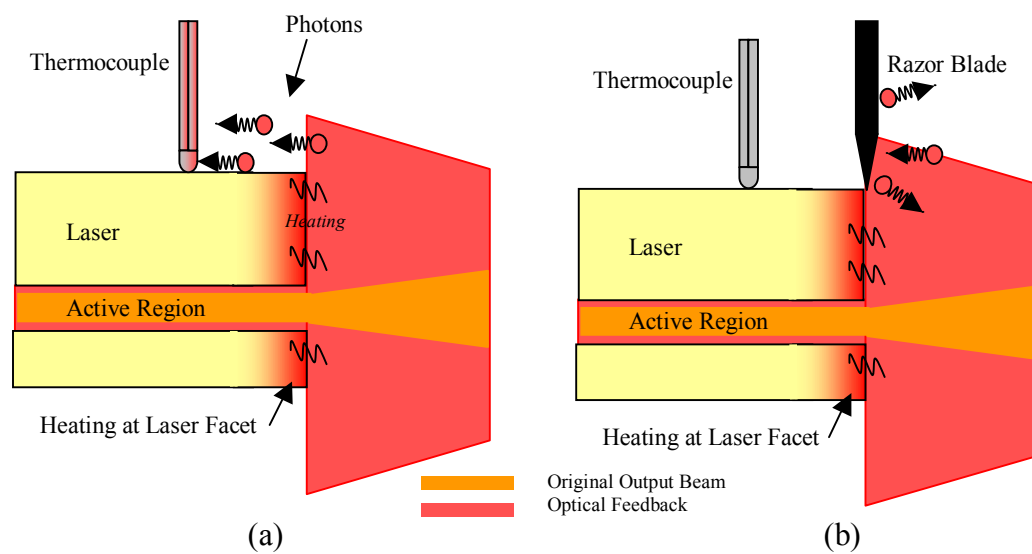


**Figure 31 - Detail of back reflected light's affect on the laser surface**

Initially we attempted to correct for this problem by being more precise in our optical alignment; this produced little change. We then attempted to move the thermocouples to the back of the device, still producing little change. The ultimate solution lay in a black painted razor blade. We positioned the razor blade just above the laser surface to prevent excess back reflected photons from striking the thermocouples. We found this technique was most effective when the razor was positioned extremely close to the actual lasing facet, as shown in Figure 33(b).

## Chapter 4 – RESULTS

### 4.1 – Quantifying the Shift in Threshold Current using Thermal Profiling

From our previous discussions of the thermal behavior of EEL, we should see cooling of the laser when it is biased above threshold. In our experimental data, we observed a linear increase in the change in temperature ( $\Delta T$ ) below threshold as current was increased, followed by a decrease in slope as photons were emitted, taking heat away from the system. This phenomena is seen in Figure 34.

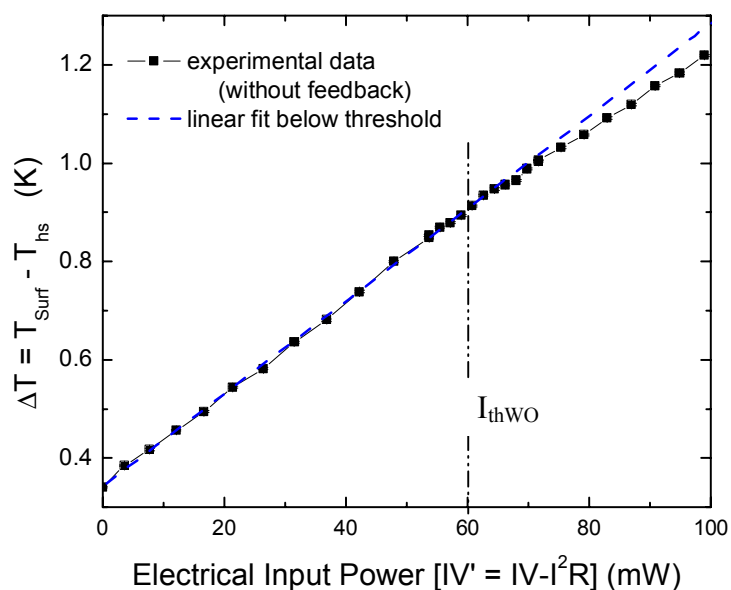
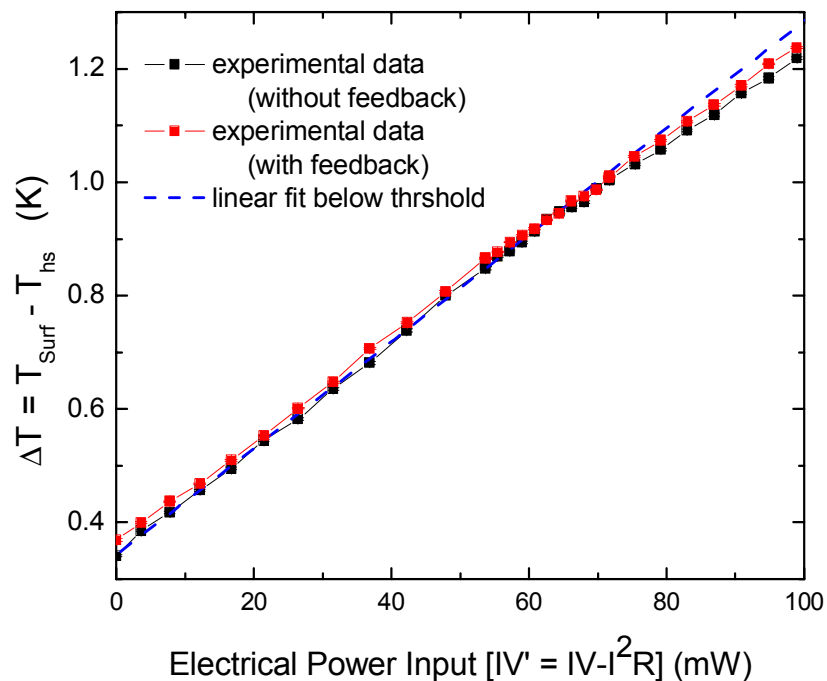


Figure 32 - Change in Temperature vs Electrical Power for the without Feedback Case

By adding optical feedback to the laser, we expect that more photons will leave the cavity, taking more heat away from the system, producing additional cooling. Unfortunately, this phenomena is difficult to observe since not all of the back reflected light gets coupled into the laser cavity. The extra light is absorbed by the front facet of the laser and causes additional heating of the device. Therefore, in our experimental data in the with feedback case, we observed cooling above threshold, although not enough to surpass the without feedback case, shown in Figure 35.



**Figure 33 - Change in Temperature vs Electrical Power  
- With and Without Feedback Cases**

By closely observing Figure 35, one can see the clear demarcation where the thermal measurements fall away from the linear fit. This point is of particular interest since lasers exposed to optical feedback will reach threshold before lasers without. Therefore if we hope to prove that thermal measurements can be used to detect optical feedback, we should observe a threshold shift in the thermal data. In order to highlight this point we have graphed  $\Delta T$ 's deviation from the linear fit below threshold for with and without feedback in Figure 36.

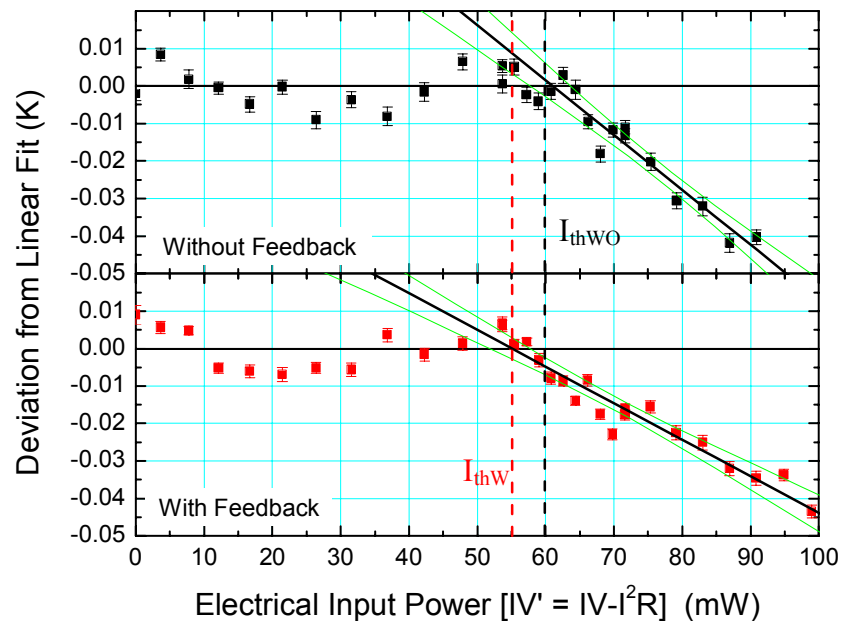


**Figure 34 - Deviation from the Linear Fit - With and Without Feedback**

In Figure 36, the black line is the linear fit of the data above threshold, while the green lines are the corresponding confidence bands. By observing this graph it is apparent that we do have a shift in threshold with feedback. In this graph we see that the threshold current without feedback is  $I_{thWO-temp} = 60 \pm 2.25$  mW, while the threshold current with feedback is  $I_{thW-temp} = 55 \pm 2.25$  mW. With quantitative

numbers for threshold currents from our thermal data we can compare these to our direct optical data. In Figure 37, we have graphed the optical output power (both the directly measured<sup>6</sup> and thermally calculated) versus the electrical input power for the with and without feedback cases.

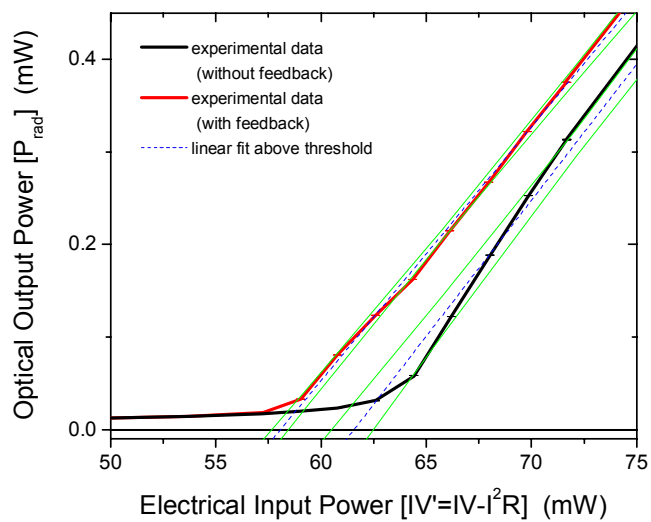


**Figure 35 - Optical Output Power vs Electrical Input Power**

On this graph we see the clear threshold shift and the corresponding threshold currents. We find threshold current with feedback is  $I_{thW} = 58.0 \pm 0.5$  mW, while threshold current for the without feedback case is  $I_{thWO} = 61.5 \pm 1.0$  mW. A summary of our observed threshold input powers for the optical and thermal data are shown in Table 1.

Table 1 – Observed Threshold Input Powers		
	Thermal	Optical
Without Feedback	$60 \pm 2.25$ mW	$61.5 \pm 1.0$ mW
With Feedback	$55 \pm 2.25$ mW	$58.0 \pm 0.5$ mW

At this point we are already beginning to see how successful thermal measurements are in the measurement of optical feedback. In order to strengthen this argument we prove how by using thermal measurements in conjunction with total energy balance model, we can solve for optical output power ( $P_{out}$ ).

#### 4.2 – Predicting Optical Output Power from Thermal Measurement

In chapter 2, we studied the external heat exchange model in detail and found that it was easily adapted for thermal applications. Now it is time to put that equation to use, in order to solve for optical output power ( $P_{out}$ ). Rearranging the terms in equation (11) we can set  $P_{rad}$  equal to our experimental terms.

$$P_{rad} = IV' - \frac{T_{surf} - T_{hs}}{Z_T} - A_{eff}h(T_{surf} - T_{amb}) \quad (15)$$

It is important to note that  $P_{rad}$  is not the same as the total optical output power,  $P_{out}$ . Rather  $P_{rad}$  is defined as the total power lost due to emission or absorption of photons. In the without feedback case,  $P_{rad} = P_{out}$ . While in the with feedback case, we have some additional heating terms to account for, which we shall explore in detail in the next section.

Also note that the total output power of the laser,  $P_{out}$ , is not the same as the optical power measured at the photodetector ( $P_{PD}$ ).  $P_{PD}$  only accounts for a fraction of the total output power. First, EELs emit light from both ends, decreasing the amount of optical power measured by the photodetector by half. Secondly, only a fraction of that light is transmitted through the attenuators and

external reflecting mirror reaches the photodetector. In order to account for these losses we must adjust our measured output power  $P_{PD}$ :

$$P_{out} = \frac{2 * P_{PD}}{T_{MIRR} T_{ATTEN}} \quad (16)$$

In equation (16),  $P_{out}$  is the total output power of the laser.

#### **4.2.1 – Modification of External Heat Exchange Model to account for Optical Feedback**

Once optical feedback is introduced into the laser, we must redefine the total energy balance equation (11) to account for optical feedback.

The fraction of output power that is back reflected into the lasing cavity is defined as the equivalent reflectivity ( $R_{eq}$ ), which is described by the components of setup.

$$R_{eq} = T_{ATTEN}^2 R_{MIRROR} \quad (17)$$

where  $R_{MIRROR}$  is the total reflectivity of the external mirror and  $T_{ATTEN}$  is the transmittance of the attenuators included in the setup.  $T_{ATTEN}$  is squared in the above equation to account for the initial and reflected trip of the light through the feedback cavity.

The fraction of back reflected light that is successfully coupled into the lasing cavity is defined by the coupling efficiency  $\rho$ . Therefore, the fraction of the light lost as additional heating around the laser facet is  $(1-\rho)$ . Combining

these elements we can define the total optical output power for optical feedback as:

$$P_{rad} = P_{out} - P_{out}R_{eq}(1 - \rho) \quad (18)$$

where  $P_{out}$  is the total optical power emitted from the laser. When we add this to our total energy balance equation (11) and arrange the terms so that the heating terms are on the left hand side of the equation and the cooling on the other, we are left with the total energy balance equation under the influence of optical feedback:

$$P_{out}R_{eq}(1 - \rho) + IV' = \frac{T_{surf} - T_{hs}}{Z_T} + A_{eff}h(T_{surf} - T_{amb}) + P_{out} \quad (19)$$

In order to use this equation to solve for  $P_{rad}$ , we must solve for it in equation (19), resulting in:

$$P_{out} = \frac{IV' - \frac{T_{surf} - T_{hs}}{Z_T} - A_{eff}h(T_{surf} - T_{amb})}{(\rho * R_{eq}) - (R_{eq} + 1)} \quad (20)$$

#### 4.2.2 – Calculating Thermal Impedance ( $Z_t$ )

Before solving for the output power ( $P_{rad}$ ) we must first solve for  $Z_t$  and  $A_{eff}h$ .

Remember back to Chapter 2, we can solve for  $Z_t$  and  $A_{eff}h$  using

$$A_{eff}h = \frac{\Delta T_0}{Z_t(T_{amb} - T_{surf})_0} \quad (10)$$

$$Z_t IV' = \Delta T - \frac{\Delta T_0}{(T_{surf} - T_{amb})_0} (T_{surf} - T_{amb}) \quad (11)$$

and plotting  $\Delta T - \frac{\Delta T_0}{(T_{surf} - T_{amb})_0} (T_{surf} - T_{amb})$  versus  $IV'$  below threshold.

Figure 38 contains our experimental data for  $Z_t$  for laser #2. Calculating the slope of the linear fit below threshold for Figure 38, we find  $Z_t = 17.94$  K/W. With this value in hand, we use equation (10) to solve for  $A_{eff}h = 6.98$  mW/K.

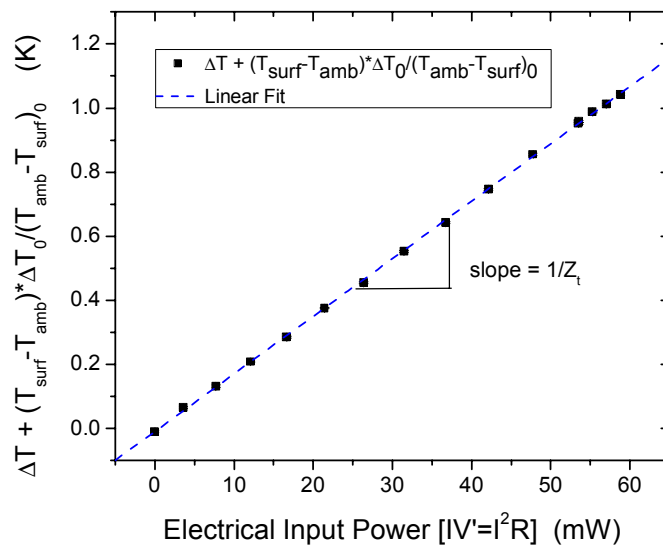


Figure 36 - Calculations for the Thermal Impedance of laser #2

#### 4.2.3 – Direct optical measurement of Optical Output Power ( $P_{out}$ )

Taking our experimental values,  $Z_t$ , and  $A_{eff}h$  and placing them into equations

(15) and (20) for without and with feedback respectively, we were able to

calculate the optical output power ( $P_{out}$ ) versus  $IV'$  for our thermal data. In Figure

39 we have graphed our calculated  $P_{out}$  along with our direct optical measurements and found a convincing agreement.

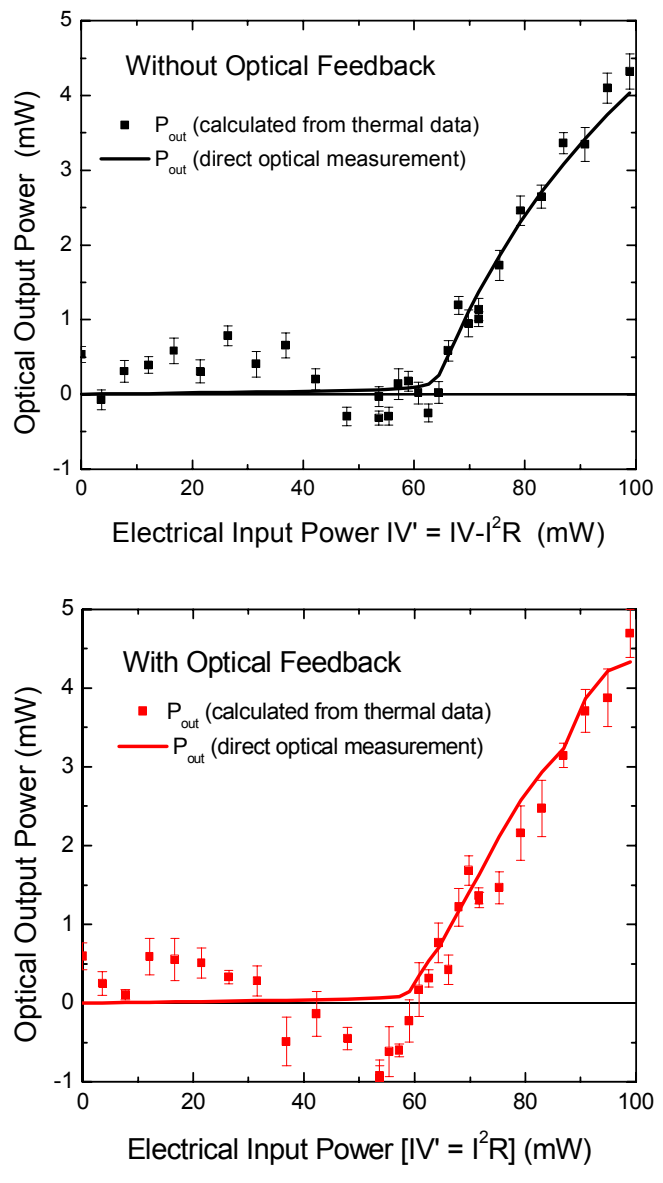


Figure 37 - Calculated Optical Output Power vs Direct Optical Measurements  
- With and Without Feedback

Difficulty in producing Figure 39 occurs when back reflected light strikes the thermocouples producing excess heating as discussed in section 3.2.3. If enough light is being reflected onto the thermocouples that  $\Delta T$  shows significant heating above threshold, our calculations from the thermal measurements will result in a negative value for  $P_{out}$  although the kink at threshold will remain in the same location.

From the information provided in Table 1 and Figure 39, it is apparent that we can accurately predict optical feedback with thermal profiling. But in the labs at Mount Holyoke College and the scientific community at large this is not enough. To further strength this proof, it is important to test this hypothesis for various amounts of optical feedback.

### 4.3 – Quantifying Optical Feedback with various amounts of Optical Feedback

In this section we will prove that thermal profiling is an effective technique for measuring optical feedback levels as low as 2% of the original output beam power. In order to achieve this we introduced six attenuators to our experimental setup.

Attenuator Number (Atten#)	Transmission	$R_{eq}$
Atten01	0.766	0.537
Atten02	0.448	0.183
Atten03	0.437	0.174
Atten04	0.217	0.043
Atten05	0.189	0.033
Atten06	0.101	0.009

The attenuators ranged in transmission values as shown in Table 2.

Various problem arose during the attenuator testing, the most problematic was thermocouple heating, a problem never solved due to time constraints. Therefore, we will focus on quantifying threshold shift since it does not depend on the appearance of cooling above threshold for accurate results. With a range of threshold current we can solve for the coupling efficiency ( $\rho$ ) for experimental setup #1.

Let us begin by examining the direct optical measurements for  $P_{out}$  for each of the various attenuators, shown in Figure 40. As the amount of transmission decreases for each consecutive attenuator there is less and less optical feedback in the system.

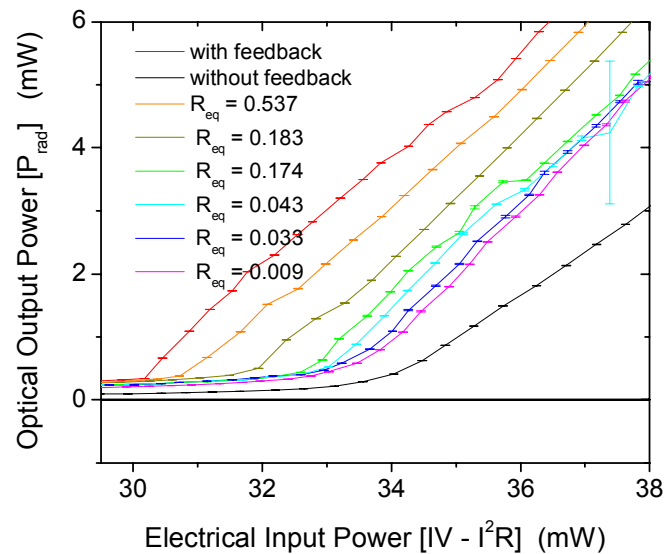


**Figure 38 - Optical Output Power vs Electrical Input Power for various amounts of Optical Feedback**

By observing the graph of  $\Delta T$  for the various attenuators, Figure 41, there is a clear place where each observation deviates from the linear fit.

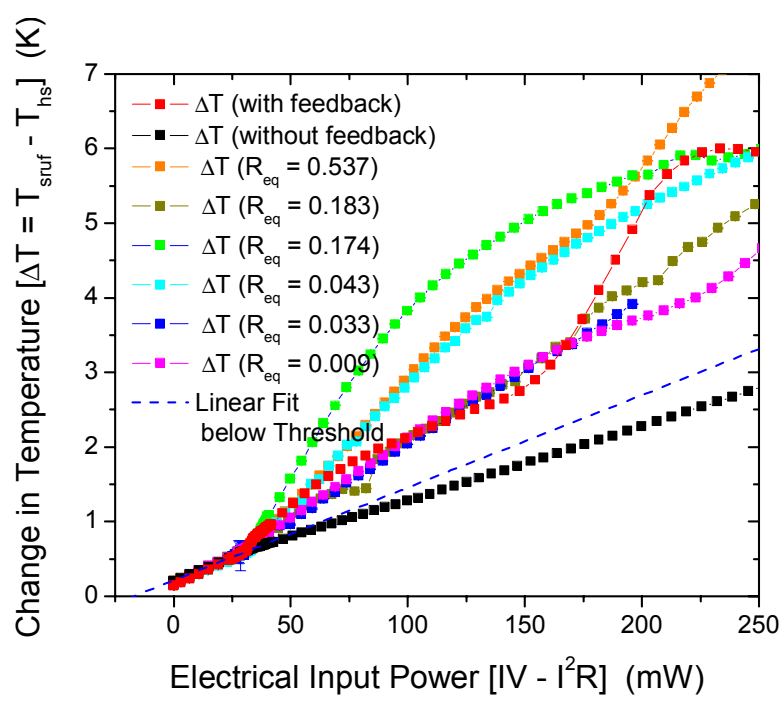


**Figure 39 - Change in Temperature vs Electrical Input Power for various amounts of Optical Feedback**

Unfortunately with optical feedback the measured temperature rises above threshold rather than cooling, pointing to back reflected light striking the thermocouples. We can investigate these lines further by graphing each one's deviation from the linear fit. For simplicity only the attenuator #2's deviation of from the linear fit is shown in Figure 42.

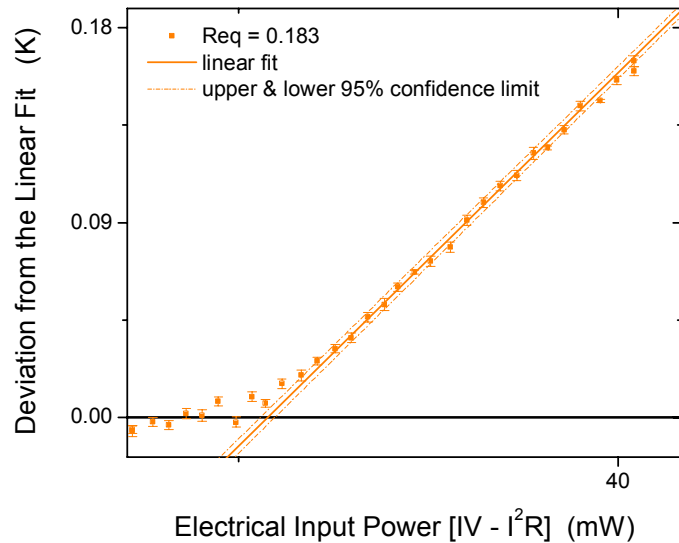


**Figure 40 - Deviation from the Linear Fit vs Electrical Input Power for Attenuator #2**

From the above figure, we can easily measure the threshold current from our thermal data. The threshold current for the additional attenuators can be found by repeating the procedure described above for attenuator #2. A summary of the threshold currents observed thermally and optically is shown in Table 3.

Table 3 – Observed Threshold Currents with Attenuators		
	Thermal	Optical
With Feedback	$30.3 \pm 0.2$ mW	$29.8 \pm 0.1$ mW
Atten01	$30.6 \pm 0.16$ mW	$30.4 \pm 0.1$ mW
Atten02	$31.5 \pm 0.16$ mW	$31.6 \pm 0.1$ mW
Atten03	$31.8 \pm 0.1$ mW	$32.2 \pm 0.14$ mW
Atten04	$32.6 \pm 0.3$ mW	$32.4 \pm 0.12$ mW
Atten05	$32.7 \pm 0.4$ mW	$32.9 \pm 0.1$ mW
Atten06	$32.9 \pm 0.2$ mW	$33.05 \pm 0.1$ mW
Without Feedback	$33.15 \pm 0.4$ mW	$33.6 \pm 0.1$ mW

The remarkable thing about this section of our research is our ability to easily extract the threshold current from our temperature measurements despite the excessive heating for these measurements, which prevented us from solving for  $P_{out}$  experimentally.

#### 4.4 – Solving for the Couple Efficiency ( $\rho$ )

In a paper written by Shijun Jiang in 1994 entitled “Influence of External Optical Feedback on Threshold and Spectral Characteristics of Vertical-Cavity Surface-Emitting Lasers,” he formulated a model for the shift in threshold current due to optical feedback:

$$\frac{I_{th}}{I_{th0}} = \frac{2\alpha l - \ln(R_1 R_{eff})}{2\alpha l - \ln(R_1 R_2)} \quad (21)$$

where  $I_{th0}$  is the threshold current of the laser without feedback,  $\alpha$  is the absorption and scattering losses inside the cavity, and  $l$  is the length of the laser cavity [2].  $R_1$  and  $R_2$  are the reflectivities of the laser mirrors, and  $R_{eff}$  is the effective reflectivity of the extended-cavity measured at the output mirror of the laser.  $R_{eff}$  was previously defined in section 2.2.1.2 as:

$$R_{eff} = \left( \frac{\sqrt{R_2} + \sqrt{R}}{1 + \sqrt{R_2 R}} \right)^2 \quad (7)$$

where  $R$  is the fraction of back reflected light:

$$R = \frac{P_{reflec}}{P_{rad}} = \rho^2 R_{eq} = \rho^2 (T_{Atten}^2 R_{Mirr}) \quad (23)$$

The variables  $\alpha$ ,  $l$ ,  $R_1$ , and  $R_2$  are relatively standard parameters for semiconductor edge emitting lasers [1]. From the literature, we use the standard values of  $\alpha l = 0.125$  and  $\sqrt{R_1 R_2} = 0.32$  for our calculation of the feedback ratio. Equation (21) is important because it relates threshold shift to coupling efficiency ( $\rho$ ) [7].

In Figure 43, we plot the feedback ratio versus the equivalent reflectivity,  $R_{eq}$ , for our each of threshold currents. The figure shows both the shift in threshold currents obtained from direct optical measurements in Figure 40, and our threshold currents determined from our temperature measurements in Figure 42. We can solve for  $\rho$  by fitting equation (21) to the experimental data, using  $\rho$  as a fitting parameter.

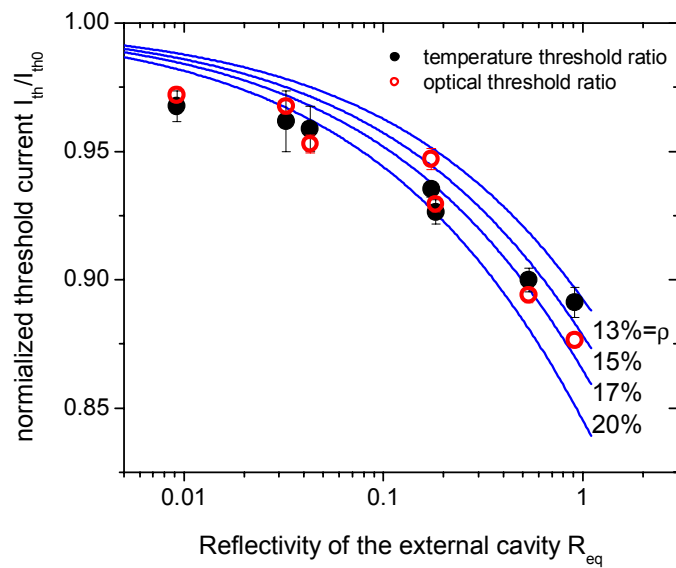


**Figure 41 - Using the feedback ratio to solve for  $\rho$**

From Figure 43, we are about extract the value for the feedback coupling efficiency for our particular setup. With this value we can quantify the fraction of back-reflected light which is coupled back into the lasing cavity.

## Chapter 5 – CONCLUSION

The purpose of our research was to examine the effect of optical feedback on the thermal characteristics of edge-emitting semiconductor lasers. In doing so we proved that it is possible to accurately quantify the optical output power of a laser with and without optical feedback. To accomplish this, we first had to modify the total energy balance equation to account for the presence of optical feedback. However, we also found that obtaining the measurements required to solve for the optical output power thermally was extremely difficult. This was due to the back-reflected light striking the thermocouples creating an erroneously high value for  $\Delta T$ .

Fortunately, we have also shown a way of working around this problem by focusing on our ability to accurately measure the shift in threshold current through thermal profiling. Threshold currents found experimentally were used in conjunction with a modification of the model described by Olsson and Jiang, in order to both quantify the total amount of optical feedback affecting an EEL and calculate the optical feedback coupling efficiency,  $\rho$  [4,1].

As a result, we have provided two sound methods for quantifying optical feedback in EELs using thermal profiling. We can calculate the optical output power directly from the total energy balance equation. Alternatively we can measure the shift in threshold current and use the modified model developed by Olsson and Jiang to derive the optical output power.

By proving that we can accurately quantify minute levels of optical feedback (as small as 1.34%) through thermal observations alone, we have provided a non-invasive technique for monitoring optical output power. This technique can now be implemented for use with devices which do not allow for direct optical access such as photonic integrated circuits.

This technique will also open the door to a variety of new research topics, in which optical phenomena can be studied using thermal measurements.

## Appendix A – Thermocouple Construction Guide

The critical component of accurate thermal measurements is a set of well constructed micro-thermocouples. For our experiment, good construction is defined as two (or more) thermocouples that read to within  $0.1^{\circ}\text{C}$  of one another while measuring temperature of a thermally controlled device such as a heat sink.

However, this level of precision is easy to

obtain once we realize that *good thermocouple construction is wholly dependent on the soldered tip.*

There are a number of reasons why two thermocouples can produce dissimilar readings. The first lies in simple placement; any changes in the angle at which the thermocouple is placed on the device can significantly change the measured temperature, depicted in Figure 44.

The larger the tip the more sensitive the thermocouple is to slight variations in the lean angle. Second, differing thicknesses in solder on one thermocouple tip

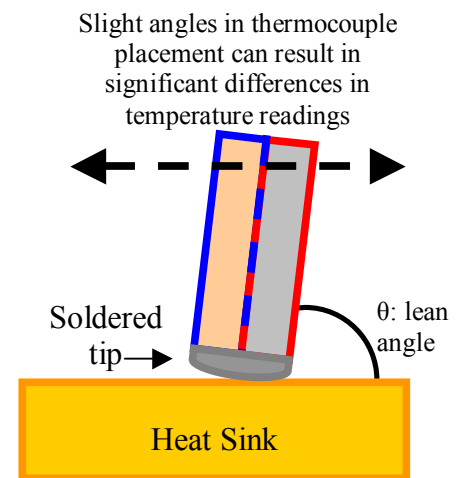


**Figure 41 - Micro-thermocouple placement on a temperature controlled device**

compared to another can produce significantly different measurement readings. From the above complications, the necessity for a thin, consistently made thermocouple tip becomes obvious.

### **A.1 – Thermocouple Construction**

A thermocouple is made up of two wires that are soldered together at the end. In our lab, two different thicknesses of thermocouple wire were used; a thick thermocouple wire which is connected to a plug for the thermocouple box, and the precision thermocouple, which is smaller than a human hair, see Figure 45. For our experiment we used copper-constantan thermocouples from Sable Systems.

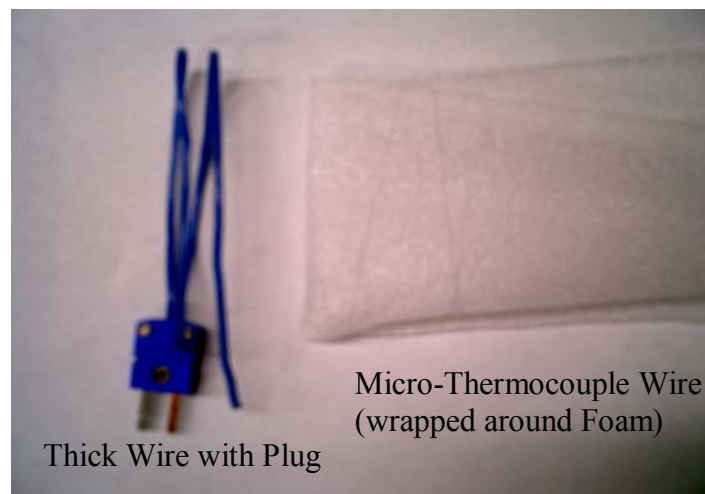


**Figure 45 - Thermocouple Wires**

In order to work in lab, these two wires must be soldered together. We begin by removing the insulation from one end of both types of wire. For the

thick wire, one can simply take the soldering iron to the exterior plastic and melt away a section in order to make it easier pull the desired length of insulation off.

Insulation removal for the thin thermocouple wire is much more difficult. For this pair of wires, the most important thing is to separate the two wire. We can do this by melting the insulation away by running one end of the wire through an open flame (typically from a cigarette lighter).

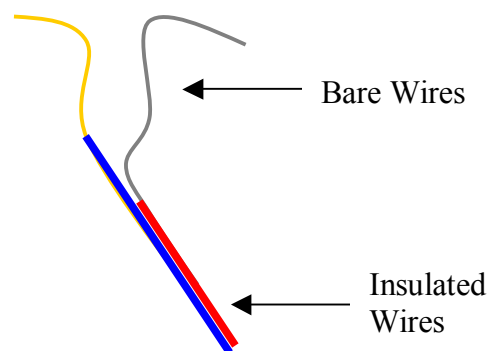


**Figure 46 - Bare Micro-thermocouple**

Once this is done, simply scrape away the charred section with your finger nail. In doing so look for two small wire ends, like the ones shown in Figure 46. Now carefully pull on these wires in order to separate the wires further. (Note: the fact that most of the wire is still covered in insulation is fine, since the remaining insulation will be removed during soldering.)

With both types of thermocouple wire separated, one can now solder them together. The easiest method is to wrap the micro-thermocouple wire around a loop of the bare thick thermocouple wire, as shown in Figure 48. Remember that when creating these loops to wrap the copper micro-thermocouple wire around the thick copper wire, and the *constantan* micro-thermocouple wire around the thick *constantan* wire, or the device will not work as a thermocouple. The wires can be easily distinguished by their bare wire color, copper will have an orange

color while constantan is silver. Soldering of this junction should be done at a temperature ranging from 750°-780° F.

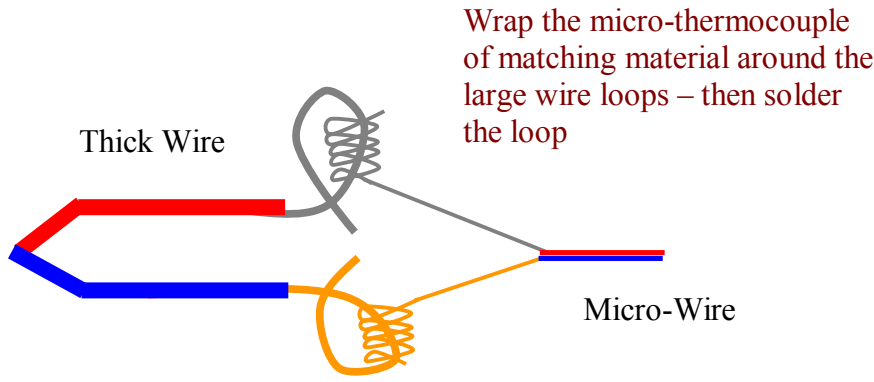


**Figure 47 - Thermocouple Wrappings**

This arrangement ensures that the micro-thermocouple wire will be held in place until it can be soldered. In order to protect this delicate junction, simply form a protective sandwich for it with some electrical tape, like the one shown in Figure 48.

In order to test the junction, put a dab of solder onto the end of the micro-thermocouple, and attach the plug to a multimeter. If you experience a short on open, go back and resolder the junction; testing this junction now will save one time and headaches later.

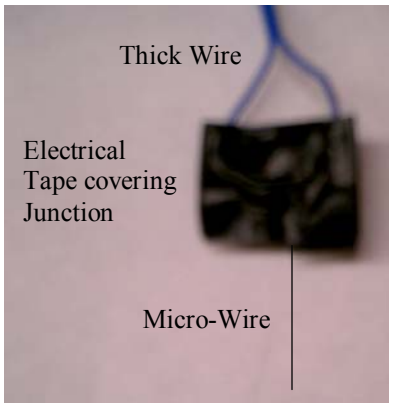


**Figure 48 - Soldering Junction Protection**

At this point, it is a good idea to mount your thermocouple onto a micro-positioner (or similar device), which will be used to position your thermocouple during the experiment, as seen in Figure 49. This will help to stabilize the tip during soldering, as well as protecting your wires from accidentally snapping during the construction of the thermocouple tip.

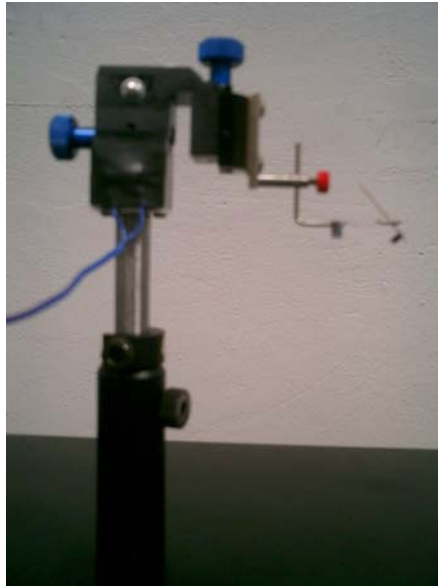


**Figure 49 - Thermocouple on a Micro-Positioner**

### **A.2 – Tip Technique**

Now that the thermocouple is created and mounted on a micro-positioner, cut off the test tip and place the thermocouple under a microscope so that the tip can be seen easily. Also increase the temperature of the soldering iron to between 810°-820° F.

Now zoom in on the thermocouple tip, load the soldering iron with solder, and move the soldering iron into the viewing area under the microscope. Now with reptilian slowness, touch one of the outside edges of the solder (yes just the edge of the solder) to the tip of the thermocouple and remove it. If done correctly, there should be a thin line of solder across the front edge of the device. A schematic of this procedure is shown

in Figure 50. If one sees any large uneven blob of solder on the tip, simply cut off the tip and try again. It is very important that the tip is nothing more than a thin even strip across the two wires.

At this point, it is important to test the thermocouple again. Testing of the thermocouple is important because there are times when solder is on the tip but not making a clean connection, leaving an open circuit. We found it handy to just leave the multimeter connected to the thermocouple during tip soldering, in order to allow for quick reference. A

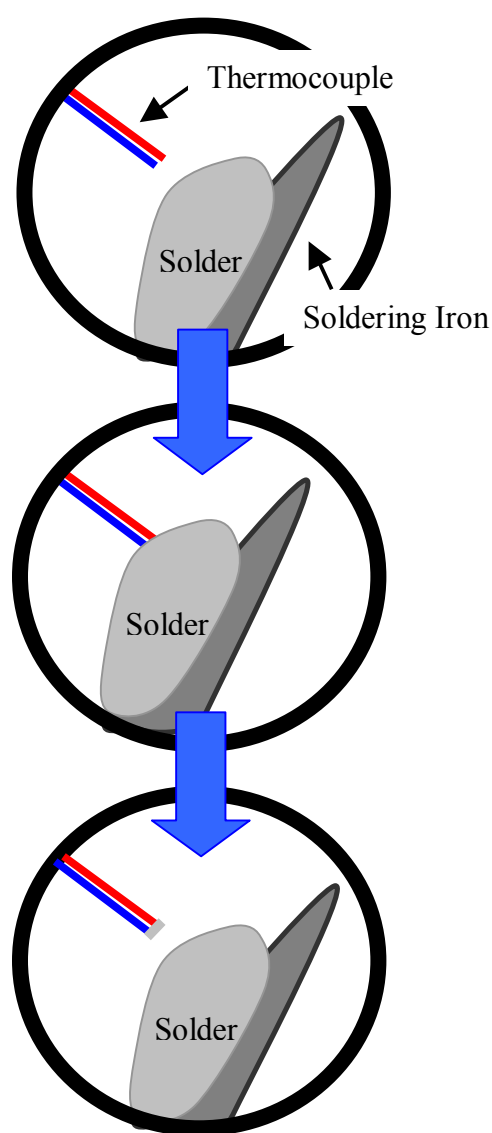


Figure 50 - Schematic of Tip Creation

good thermocouple should have a resistance ranging between 150  $\Omega$  – 500  $\Omega$ .

### A.3 – Application of Electrical Insulation

The final step in the successful completion of thermocouple construction is in the application of super glue to the thermocouple tip in order to prevent the thermocouple from picking up unwanted current off the laser (or any other device being measured).

Place the thermocouple under the microscope again and zoom in on the tip. Now squeeze the super glue so a small bubble forms at the tip of the tube of super glue and move it into the viewing area under the microscope.

Similar to the technique used with the soldering iron, simply dab the tip into the super glue. This should leave a series of small bubbles along the length of the tip due to the natural properties of the material, as shown in Figure 51.

To create an even coating over the tip, take a small pair of tweezers

and smooth the glue over the tip. This should leave a series of small bubbles along the length of the tip due to the natural properties of the material, as shown in Figure 51.

To create an even coating over the tip, take a small pair of tweezers and smooth the glue over the

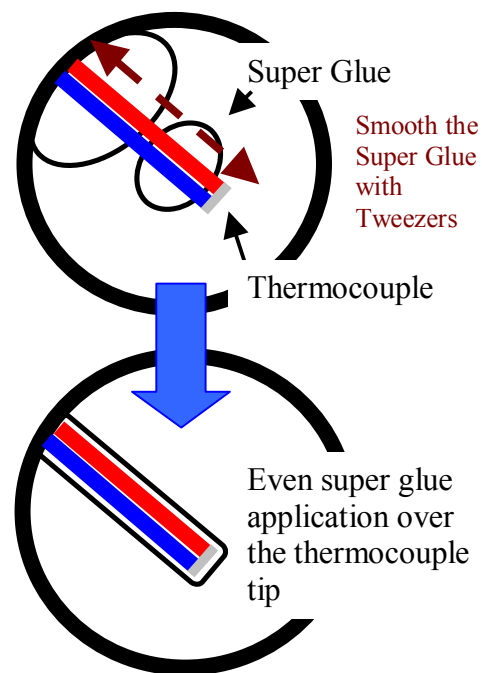


Figure 41 - Application of Super Glue

length of the thermocouple making sure to pull the glue down over the metal tip, since that is the area we need to cover, see Figure 51.

Once the tip is covered, let it dry of a few minutes, and then test the resistance. This is done by attaching one end of the multimeter to one of the plug ends and a probe to the other. This probe can be any metal object that can be connected to the multimeter and run across the tip. We typically used a wire pin that was held by a multimeter attachment, as shown in Figure 52.



**Figure 52 – Probe used to test Thermocouple Resistance**

The resistance was then tested by rolling the probe across the surface of the thermocouple tip. Be sure to roll the probe all the way around the thermocouple tip, watching the multimeter closely, since a tip has been shown to be insulated in some area and not in others. If the circuit is shorted out during this test, the thermocouple has been correctly coated, since we do not want an electrical current to flow through the tip with the coating present.

Following this technique, one should be able to produce nicely constructed thermocouples, due to careful creation of the soldered tip.

#### **A.4 – Thermocouple Testing**

Once both thermocouples have been constructed, it is time to test the thermocouples to see if they match to within 0.1°C. This is a fairly simple procedure.

Begin by plugging the thermocouples into the Sable Systems thermocouple box and connecting it to the computer. This box employs an internal reference temperature and the Seebeck Effect to calculate the thermocouple temperatures from their voltage.

The first test is to take both thermocouple tips at the same time and hold them near to one another between your thumb and index finger. Squeezing your fingers together around the thermocouple tips should result in very similar readings although not 0.1°C. If the two temperatures are reading very differently, go back and reconstruct the tip of one of the thermocouples.

Once the thermocouples have passed the first test, place them close together, but not touching, on a heat sink set between 18°-20°C. The positioning of the thermocouples on the heat sink should be done under a microscope in order to ensure that the tips are placed close to one another and setting upright on the heat sink without much tilt, as shown in Figure 44. Once the thermocouple is resting on the heat sink, small adjustments to the thermocouples, tilt position can be made with the micro-positioner in order to get the thermocouples to read more closely. However, if the tips are carefully constructed this will not be an issue.

Once the thermocouples are placed in a satisfactory manner, this may take sometime to achieve, turn off the microscope light and carefully place a dark blanket over the experimental setup being careful not to knock the thermocouples out of place. This process is called ‘ghosting.’ With the experimental setup ghosted, observe the thermocouple readings over time, at this time they should be reading within  $0.1^{\circ}\text{C}$ . The easiest way to observe the difference in temperature between the thermocouples is to write a LabView code which plots the thermocouple temperature difference as  $(T_1 - T_2)$  as a function of time. Once two (or more) thermocouples have been constructed that read within  $0.1^{\circ}\text{C}$  of one another, thermocouple construction is complete.

**REFERENCES:**

- [1] S. Jiang, et al, "Influence of external optical feedback on threshold and spectral characteristics of VCSELs," *IEEE Photonic Technology Letter*, vol. 6 34-36, 1994.
- [2] C.H.L. Quay, I.Z. Maxwell, and J.A. Hudgings, "Coherence Collapse and Redshifting in Vertical-Cavity Surface-Emitting Lasers Exposed to Strong Optical Feedback," *Journal of Applied Physics*, vol. 90, 2001.
- [3] Petermann, Klaus. "External Optical Feedback Phenomena in Semiconductor Lasers," *IEEE Journal of Selected Topics in Quantum Electronics*, vol. 1 no.2, pp. 480-489, June 1995.
- [4] A.Olsson and C.L. Tang, "Coherent Optical Interference Effects in External-cavity Semiconductor Lasers," *IEEE Journal of Quantum Electronics*, vol. QE-17, no.8, pp. 1320-1323, August 1981.
- [5] *Merriam-Webster's Medical Desk Dictionary* (2005, April). [Online]. Available: <http://www.dictionary.com>
- [6] Breck Hitz, J.J. Ewing, and Jeff Hecht, *Introduction to Laser Technology* (3<sup>rd</sup> Ed), IEEE Press, New York, 2001.
- [7] L.A. Coldren and S.W. Corzine, *Diode Lasers and Photonic Integrated Circuits*, John Wiley and Sons, New York, 1995.
- [8] Bahaa Saleh, and Malvin Carl Teich, *Fundamentals of Photonics*, John Wiley and Sons, Canada, 1991.
- [9] Goldberg, Lew. "Spectral Characteristics of Semiconductor Lasers with Optical Feedback," *IEEE Journal of Quantum Electronics*, vol. QE-18, no.4, pp. 555-563, April 1982.
- [10] Lenstra, Daan. "Coherence Collapse in Single-Mode Semiconductor Lasers due to Optical Feedback," *IEEE Journal of Quantum Electronics*, vol. QE-21, no.6, pp. 674-679, June 1985.

- [11] Lang, Roy. "External Optical Feedback Effects on Semiconductor Injection Laser Properties," *IEEE Journal of Quantum Electronics*, vol. QE-16, no.3, pp. 347-355, March 1980.
- [12] Pipe, K.P. and Ram, R.J, "Comprehensive heat exchange model for a semiconductor laser diode," *IEEE Photon. Tech. Letters*, vol.14, pp. 504-506, 2003.
- [13] Hepburn, Carl. (2005, April). *Brittany Spear's Semiconductor Page* [Online]. Available: <http://britneyspears.ac/lasers.htm>